NAVAL POSTGRADUATE SCHOOL

MONTEREY, CALIFORNIA

THESIS

DESIGN AND PROTOTYPING OF A SATELLITE ANTENNA SLEW TESTBED

by

Gregory M. Contreras

December 2013

Thesis Co-Advisors: Mark Karpenko
                                                       I. M. Ross

Approved for public release; distribution is unlimited

THIS PAGE INTENTIONALLY LEFT BLANK

REPORT DOCUMENTATION PAGE		*Form Approved OMB No. 0704-0188*
Public reporting burden for this collection of information is estimated to average 1 hour per response, including the time for reviewing instruction, searching existing data sources, gathering and maintaining the data needed, and completing and reviewing the collection of information. Send comments regarding this burden estimate or any other aspect of this collection of information, including suggestions for reducing this burden, to Washington headquarters Services, Directorate for Information Operations and Reports, 1215 Jefferson Davis Highway, Suite 1204, Arlington, VA 22202-4302, and to the Office of Management and Budget, Paperwork Reduction Project (0704-0188) Washington DC 20503.		
1. AGENCY USE ONLY *(Leave blank)*	**2. REPORT DATE** December 2013	**3. REPORT TYPE AND DATES COVERED** Master's Thesis
4. TITLE AND SUBTITLE DESIGN AND PROTOTYPING OF A SATELLITE ANTENNA SLEW TESTBED		**5. FUNDING NUMBERS**
6. AUTHOR(S) Gregory M. Contreras		
7. PERFORMING ORGANIZATION NAME(S) AND ADDRESS(ES) Naval Postgraduate School Monterey, CA 93943-5000		**8. PERFORMING ORGANIZATION REPORT NUMBER**
9. SPONSORING /MONITORING AGENCY NAME(S) AND ADDRESS(ES) N/A		**10. SPONSORING/MONITORING AGENCY REPORT NUMBER**
11. SUPPLEMENTARY NOTES The views expressed in this thesis are those of the author and do not reflect the official policy or position of the Department of Defense or the U.S. government. IRB protocol number ____N/A____.		
12a. DISTRIBUTION / AVAILABILITY STATEMENT Approved for public release; distribution is unlimited		**12b. DISTRIBUTION CODE** A
13. ABSTRACT (maximum 200 words) The purpose of this thesis is to contribute to the development of the next generation slewing antennas for spacecraft, ground or sea systems. Current antenna slewing systems may also benefit from the results. More specifically this thesis provides a new testbed for implementing slew maneuvers in a laboratory environment. The antenna slew testbed was built with in-house manufactured parts, 3-D printed parts and commercial-off-the-shelf equipment. The approach for designing this testbed involved CAD analysis and rapid prototyping, the application of dynamic scaling and similitude concepts, and implementation of hardware and software to support experimentation of novel maneuver concepts. To illustrate this, a maneuver based on optimal control theory is implemented. The applicability of this testbed casts a wide net because of its scale size as compared to existing or future systems. Moreover, the testbed is designed in a modular form to allow a variety of different antenna systems to be represented for testing slews. These include ground, space, and shipboard antenna systems.		
14. SUBJECT TERMS Testbed, antenna system, optimal controls, gimbal, gimbals, testbed assembly, 3d printing, rapid prototyping, satellite antenna, slew testbed, slewing testbed		**15. NUMBER OF PAGES** 115
		16. PRICE CODE
17. SECURITY CLASSIFICATION OF REPORT Unclassified	**18. SECURITY CLASSIFICATION OF THIS PAGE** Unclassified	**19. SECURITY CLASSIFICATION OF ABSTRACT** Unclassified	**20. LIMITATION OF ABSTRACT** UU

THIS PAGE INTENTIONALLY LEFT BLANK

DESIGN AND PROTOTYPING OF A SATELLITE ANTENNA SLEW TESTBED

Gregory M. Contreras
Lieutenant, United States Navy
B.S., University of Idaho, 2007

Submitted in partial fulfillment of the
requirements for the degree of

MASTER OF SCIENCE IN ASTRONAUTICAL ENGINEERING

from the

NAVAL POSTGRADUATE SCHOOL
December 2013

Author: Gregory M. Contreras

Approved by: Mark Karpenko
                            Thesis Co-Advisor

                            I. M. Ross
                            Thesis Co-Advisor

                            Knox T. Millsaps
                            Chair, Department of Mechanical and Aerospace Engineering

THIS PAGE INTENTIONALLY LEFT BLANK

ABSTRACT

The purpose of this thesis is to contribute to the development of the next generation slewing antennas for spacecraft, ground or sea systems. Current antenna slewing systems may also benefit from the results. More specifically this thesis provides a new testbed for implementing slew maneuvers in a laboratory environment. The antenna slew testbed was built with in-house manufactured parts, 3-D printed parts and commercial-off-the-shelf equipment. The approach for designing this testbed involved CAD analysis and rapid prototyping, the application of dynamic scaling and similitude concepts, and implementation of hardware and software to support experimentation of novel maneuver concepts. To illustrate this, a maneuver based on optimal control theory is implemented. The applicability of this testbed casts a wide net because of its scale size as compared to existing or future systems. Moreover, the testbed is designed in a modular form to allow a variety of different antenna systems to be represented for testing slews. These include ground, space, and shipboard antenna systems.

THIS PAGE INTENTIONALLY LEFT BLANK

TABLE OF CONTENTS

LIST OF FIGURES

LIST OF TABLES

THIS PAGE INTENTIONALLY LEFT BLANK

LIST OF ACRONYMS AND ABBREVIATIONS

2-DOF	two degrees-of-freedom
3D	three dimensional
AZ	azimuth
BLDC	brushless DC
CAD	computer aided designs
CAN	controller area network
Cia	CAN in automation
CIWS	close in weapon system
CoM	center of mass
COTS	commercial off the shelf
cRIO	compact RIO
CSV	comma separated value
DC	direct current
DLL	dynamic link library
EL	elevation
EPOS2	easy to use POSitioning 2
FDM	fused deposition modeling
FPGA	field-programmable gate array
GSP	gooseneck support plate
IPM	interpolated position mode
NASA	National Aeronautics and Space Administration
NI	National Instruments
NPS	Naval Postgraduate School
P/N	part number
PC	white polycarbonate plastic
PC	personal computer
PD	proportional derivative
PDO	process data objects
PVC	polyvinyl chloride
PVT	position velocity time

QC	quadcounts
RIO	reconfigurable input output
rpm	revolutions per minute
SDO	service data objects
SF	scale factor
STL	stereo lithography
TDRS	tracking and data relay satellite
VI	virtual instruments

LIST OF SYMBOLS

θ	position
ω	angular velocity
ζ	damping coefficient
α	angular acceleration
$\dot{\omega}$	angular acceleration
$\dfrac{d\omega}{dt}$	angular acceleration
$\ddot{\theta}$	angular acceleration
T	torque
ω_n	natural frequency
k_p	proportional gain
k_d	derivative gain
I	moments of inertia
G(s)	transfer function
u	control function
e	error
t_s	settling time

THIS PAGE INTENTIONALLY LEFT BLANK

ACKNOWLEDGMENTS

"Evil Only Prevails When Good Men Do Nothing."— Edmund Burke

The development of this prototype is the culmination of the support from many people in many forms throughout my life. The opportunity of attending the Naval Postgraduate School is thanks to the United States Navy and my previous superiors and mentors. The greatest thanks go to my advisors Dr. I. M. Ross and Dr. Mark Karpenko. Their guidance, instruction, mentoring, and profound patience throughout this process has been the reason for such phenomenal results that will in many ways change the future of spacecraft development.

When creating this prototype many professors and professionals at the NPS provided advice, time and expertise to support the design and implementation. Much thanks goes to Dan Sakoda, John Bagnasco and Levi Owen for their support in the rapid prototyping, 3D printing and machining. The entire 591 Staff curriculum and Dr. Frank Giraldo, which wholly provided the knowledge that culminated in a masterpiece thesis; specifically Dr. Jennifer Rhatigan and Capt. Stephen Frick who always knew when to ask "how's it going" and acquire the contacts at NASA.

To the industry professionals who hurried, replied quickly, and provided their professional support beyond my requests. Especially, the engineers at Nelson Air, Biren Patel and team at Maxon Motors, and product engineers at National Instruments. A special thanks to Eva Carrillo and the TDRS team at Boeing for providing crucial data.

To my thesis partners Rich "Lifestyle" Gargano and Adam "Spill-Proof" Sears for the past 28 months in brilliance, technical support and, most importantly, their friendship. My success while in graduate school is greatly contributed to them and the Space Bears team.

To my neighbors here in Seaside, the beers and kind advice gave me a family away from home. To my familia here in the Bay Area; their constant support, understanding and surprise visits kept me motivated during my time here. Most importantly, to my girlfriend Lindsay who was always there to smile and nod kindly as I

babbled about this thesis and sacrificed her time to support these endeavors. And without question, I thank the Lord my God for the inspiration for all that I do. I dedicate this thesis to Sr. Maria Romero and Sr. Sharon MacMillan of San Carlos Cathedral for their kindness and support during my time in Monterey.

"For where two or three have gathered together in My name, I am there in their midst"—Mt 18, 20

As Always, Go Oakland!

I.   INTRODUCTION

A.   MOTIVATION

1.   Current Antenna and Multi-Axis Gimbal Systems

The concept of antenna systems has been around since the invention of radio, a term adopted by the U.S. Navy in 1912. Antenna systems now exist on a variety of platforms such as spacecraft, ground communications, and sea systems. The purpose of antenna systems is usually for signal reception or transmission. Still, any system with elevation and azimuth gimbals can provide a wider variety of uses. A multi-axis system could be used for optics and imagery, signals, weapons systems, or robotics. Current multi-axis systems, specifically space multi-axis systems have been incredibly resilient with demand for usage. Communication satellites are in high demand and on-orbit systems still struggle with meeting customer requests. Improvement upon communication antenna systems transmission traffic could be done in two ways: 1. Flight software updates or 2. Replace hardware. The goal is to improve antenna communications for more customer usage and sharing with a need for less spacecraft. Since communication satellites are typically in geosynchronous orbit, the latter is impossible or very expensive. Thus, the best way to improve communication satellite coverage is to develop upon the existing flight software. By reducing time in gimbal maneuvers an antenna slew can provide more coverage. More coverage means more products for the end-user. However, flight software changes cannot always be tested on-orbit; therefore building a system, in a laboratory environment to test improvements and enhancements to flight software would be ideal.

Altering flight software suggests altering the slewing software (commands) of the communications antenna system that provides coverage to the user. The testbed motivation is the improvement of multi-axis testbed is beneficial because, reduced cost associated with testing multi-axis systems on orbit and current systems are over-engineered and have been out living their estimated orbit design life [1], therefore instead of replacing systems that are still useful with new and expensive equipment, it would be

1

efficient to improve upon the flight software with patches. Furthermore, costs associated with testing multi-axis systems on-orbit spacecraft or on the ground are very high and interfere with meeting customer needs. So it behooves engineers to produce a physical system to develop and test the improved flight software trajectories in a laboratory environment.

2. Past Antenna Systems and Future Designs

As engineers develop the future slewing antenna systems on spacecraft, ground systems or sea systems it is industry standard to look back at legacy hardware and software and improve upon them. This thesis does not discourage improving upon legacy equipment, but rather recommends an alternative to developing flight software by building and testing an antenna testbed in a lab to test new or improved antenna slews.

B. THESIS OUTLINE AND SCOPE

Conducting slew maneuvers on on-orbit antenna systems is costly and impedes normal operations. There are similar challenges to operating ground system antennas on Earth that may be only used sparingly. The excessive amount of time spent by humans preparing trajectories for customer demands makes the cost of the operations high. To minimize cost and time required for trajectory planning, and also to maximize the mission effectiveness by reducing wasted time, a tool to assist in trajectory planning and testing is required. Building a slewing antenna testbed is one approach towards accomplishing this goal. This approach can help to provide feasible and implementable solutions to antenna motion/path planning problems that maximize mission relevant objective functions such as time, distance, or fuel [2]. This thesis focuses on the design, construction and testing of a slewing antenna testbed that utilizes real-time control software. Various maneuver trajectories are analyzed and implemented on the antenna testbed to demonstrate the application of the system. The scope of this thesis is limited to examining conventional linear control theory and optimal control concepts based on simple models as a means to illustrate a procedure for antenna slewing and laboratory testing that could be applied to operating and future slewing antenna systems.

The remainder of the thesis is outlined as follows: Chapter II discusses the testbed design approach and requirements that the testbed should meet. The testbed design and integration of software and hardware are described in Chapter III. Chapter IV develops several different maneuver trajectories and shows how they can be implemented on the antenna gimbals. Next, Chapter V presents some ideas for dynamic scaling of full scale systems to the laboratory testbed and illustrates of the experimental implementation of a real system to the testbed. The thesis is concluded in Chapter VI and some ideas for future are given.

THIS PAGE INTENTIONALLY LEFT BLANK

II.   TESTBED DESIGN APPROACH AND REQUIREMENTS

A.   TESTBED OVERVIEW

The purpose of this thesis is to contribute to the development and testing of antenna pointing and slew maneuver systems by designing and building a prototype with real-time controls. The design is representative of a multitude of antenna slewing platforms. The objective is to build a testbed on a short timeline, have a flexible setup, have the ability to incorporate commercial-off-the-shelf (COTS) equipment, and have the ability to implement arbitrary maneuvers with an emphasis on the dual axis gimbal assembly. The testbed is an open-architecture system. As stated by Ackman, an open-architecture system enables customizable hardware and software configuration and allows for future system upgrades, component swapping and integration with other systems [3]. This technical objective can be approached through an iterative design process in which several mechanical design configurations are explored prior to the manufacturing of the first prototype of a final testbed [3]. This iterative design process can support the need to construct and evaluate the performance of the testbed on a short, thesis driven timeline.

The final testbed will integrate various hardware, software and mechanical components. The final system is therefore a combination of COTS equipment, custom designed parts and in-house wiring. To ensure completion on a short timeline, the antenna mechanism itself may be built from computer-aided designs (CAD) manufactured using a rapid prototyping machine (three dimensional (3D) printer) then integrated into a final assembly.

The final testbed should not be confused with an initial prototype. The testbed is the working assembly of equipment that may be used to produce lab results and the design iterations lead up to an initial testbed, or prototype one. Future prototypes can be developed based on this testbed for use with slew trajectories to either better the design or increase the utility of the initial testbed. The testbed designed in this thesis will implement multi-axis gimbals, as well as concepts from control theory, and multi-body

mechanics. The testbed with its "utility" or functionality can thus mimic a variety of systems. For example, any system with an azimuth or elevation gimbal (or just a single gimbal). This includes ground, sea, aircraft or any number of significant space systems with a slewing antenna in (see Figure 1). Figure 1 (a) is a ground antenna for the deep space tracking station network from the European Space Agency; Figure 1 (b) is the Navy multiband terminal (NMT) from Raytheon Corporation, the NMT is one of three terminals in Raytheon's product line that support the Army, Navy and Air Force; Figure 1 (c) is the TDRS satellite S-Band antenna dish from Boeing Corporation.
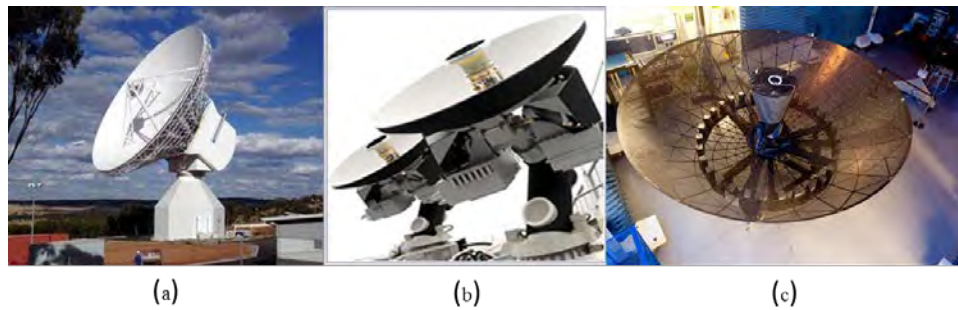
Figure 1.   Various Antenna Platforms: (a) Ground, (b) Sea, (c) Space

The requirements set forth for the testbed were: 1. Quick build; meaning the testbed had to be designed, built, and tested within a 10 month thesis timeline. 2. Flexible system; meaning the testbed had to be a modular and scalable to mimic a variety of antenna slewing platforms having an azimuth and elevation gimbal. 3. Ability to perform an arbitrary maneuver; meaning the testbed gimbals would need to maneuver (or operate) based on any given trajectory. In the next few sections, options for addressing these requirements are outlined.

B.   RAPID PROTOTYPING

The World Technology Evaluation Centers reports, "mastering the art of rapidly prototyping parts and products was vital for any corporation in the race to launch new products" [4]. Rapid prototyping can be used as part of the thesis for two reasons: One, the ability to produce several design iterations quickly; Two, the ability to design, build and test an entire testbed in less than 12 months. To address the reasons listed, a solution

was embodied as rapid prototyping. Rapid prototyping allows for turn around as soon as the designer makes changes and provides a method for manufacturing prototype parts. By having the ability to make prompt design changes and rapidly print parts, the testbed may be quickly manufactured within the thesis timeline; allowing time to build, integrate parts and conduct testing.

The Naval Postgraduate School (NPS) Space Systems Academic Group procured a Fortus 400mc rapid prototyping machine in 2008. The machine employs fused deposition modeling (FDM) for additive manufacturing of 3D parts from CAD geometry. CAD models are imported in the stereo lithography (.STL) file format to the printer software [5]. The .STL files are created from Solidworks after the part or assembly has been designed and saved as a .STL file. After orienting the part for the build, the Fortus machine software slices horizontal build planes and creates tool paths for each slice of the part based on the configuration of the machine and user-selectable parameters. Once print jobs are generated, another software application is used to arrange them on the build area and send them to the machine. In this way, time can be saved by printing a number of parts, at the same time as long as they can fit within the envelope of the machine and the build footprint [5]. By using the 3D printer, a C effector design AD model could be used to manufacture a rapidly produced or printed part. The CAD model of the current design iteration can be exported to 3D printer to produce a plastic prototype of the testbed assembly. The 3D printer thus allows for an inexpensive and quick way to test and evaluate the placement, fit and tolerances of mating parts prior to finalizing the design [3].

C.   DYNAMIC SCALING AND SIMILITUDE

The thesis requirement of a flexible system means the testbed should, within reason, be able to mimic the dynamical behavior and structure of a variety of antenna slewing platforms or systems having an azimuth and elevation gimbal. To meet this requirement of mimicking a full or real operating system, the system and its dynamics have to be scaled to the testbed. After researching methods of scaling models, as routinely done with aircraft and automobiles, it was concluded that dynamic scaling or

similitude concepts can be used to employ testbed for dynamic simulation of a real system. Reference [6] states, "Since, none of mathematic model can completely represent a real physical system; the non-exact model will result in some simulation error" furthermore "To reduce developing cost and time, recently, many researchers have developed scaled vehicles. Scaled vehicles are proportionally similitude vehicles that have similar dynamic behavior of those full size vehicles. There are several advantages of using the scaled vehicle over a full-size vehicle. The scaled vehicle is more simple and inexpensive. In addition, it is relatively simple to change testing conditions and environment. This makes the testing safe, fast, and repeatable". The same principles can be applied when developing the testbed as part of this thesis for the same benefits listed so the testbed can mimic a real system as closely as possible.

The use of dynamic scaling will be described more in depth in Chapter V. The concept of dynamic scaling is more widely known in the field of aeronautics and automobile design. Reference [7] describes that prior to the mid-1990s the use of similitude for scaled models provided benefits such as cost and time savings in operating and development in full scale aircraft and by extension a spacecraft. Recently, many researchers have developed scaled vehicles. Scaled vehicles are proportionally smaller, also called similitude; these vehicles have similar dynamic behavior of full sized vehicles. Usually smaller models mimic the behavior of full scale (with some error) but the benefit of the testbed is the flexibility to mimic various full scale antenna platforms instead of just a single full scale system. The inertia tensor matrix shown in Equation 2.1 has the 3D components of a rigid body that defines its resistance rotate about a given axis.

$$I = \begin{bmatrix} I_{xx} & -I_{xy} & -I_{xz} \\ -I_{xy} & I_{yy} & -I_{yz} \\ -I_{xz} & -I_{yz} & I_{zz} \end{bmatrix}$$

(2.1)

Dynamic scaling will consider the parameters of an antenna system, which include the inertia tensor above as well as the center of mass and center of gravity. Therefore the

scaling factor will change based on the antenna system being scaled and the properties of the testbed. A basic similitude scaling factor, SF, can be described as:

$$
\begin{bmatrix} I_{xx} & -I_{xy} & -I_{xz} \\ -I_{xy} & I_{yy} & -I_{yz} \\ -I_{xz} & -I_{yz} & I_{zz} \end{bmatrix}_{AS} = SF * \begin{bmatrix} I_{xx} & -I_{xy} & -I_{xz} \\ -I_{xy} & I_{yy} & -I_{yz} \\ -I_{xz} & -I_{yz} & I_{zz} \end{bmatrix}_{Testbed}
\tag{2.2}
$$

SF is a matrix determined for each antenna system being modeled (scaled) and is a function of mass and a function of position of the center of mass (X, Y, Z) relative to a body reference frame. As the testbed inertia tensor stays constant with the design (the inertia will change, however, with subsequent prototype iterations) the SF will change for each real world system to satisfy Equation 2.2. A secondary method described in Chapter V also introduces scaling by momentum matching.

D.   PROFILE MANEUVERS

1.   Trajectory Function

The testbed requirement of having the ability to perform an arbitrary maneuver (slew) was the primary focus of the thesis, where the testbed gimbals need to move based on any arbitrary trajectory. The maneuver could be developed using a second order polynomial, as an optimized path or simply as a set of arbitrary points forming a trajectory. The maneuverability was important to implement so as to simulate real systems either currently operational or in development (ground, sea, or space). By having a testbed with similar gimbal designs to antenna systems used all over the world, being able to test new trajectories or slews in a lab environment will ultimately save time and cost. To achieve this benefit of testing in a lab environment, hardware and software with real-time capability is needed as well as application of control theory to create the trajectory functions that can be implemented on the testbed.

A profile maneuver is described in depth in Chapter IV. In general, a profile maneuver is a best-fit nth order polynomial. On the testbed, data for the polynomial can come from an antenna system (azimuth and/or elevation gimbals being scaled or mimicked), or from the solution of a second-order system model that provides azimuth or

elevation angles versus time. The purpose is for a cubic (or higher order) spline to fit the data and be implemented into the gimbal motors as commands given in terms of degrees (or radians) to change the position. Appropriate software driving the motor controller implements the polynomial path as a table or set of data representing degrees/radians/position (motor quadrature counts) versus time. The software can upload the points to the motor controllers and cause the motors to follow the path. Figure 2 shows a polynomial function denoted by the data points (red), while the blue curve shows the interpolation polynomial of nth degree.
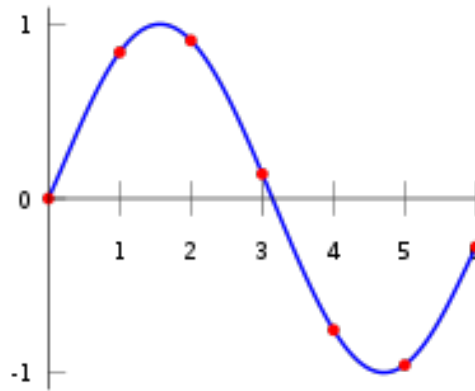
Figure 2.　Maneuver Trajectory Based On Polynomial Curve Fit

2.　Optimal Controls

The implementation of optimal control is described in depth in Chapter IV. The theory of optimal control has been implemented on a large spectrum of engineering systems. Optimal control takes the problem data and solves a control trajectory that considers all the body mechanics and dynamics of a structure and maximizes agility of that structure (or mechanical body). Optimal control can be applied to reduce time, fuel, and cost and uses boundary constraints and differential equations to establish the optimal path. Figure 3 shows an example optimal path y(t) as compared to a conventional path y*(t). Though the path for y(t) appears longer, the y(t) function may conserve fuel even though both paths completed the overall maneuver in the same amount of time.

Optimal control is implemented to reduce some performance metric that can benefit the user. By reducing time or fuel or both, the user reduces cost. Optimal control is very important in the field of space applications as to reduce time or fuel when slewing. This process, if implemented on a testbed can provide a motivation for applying this concept to any system that slews an antenna or pointing system, whether autonomous or guided/commanded. This can include, but not limited to: large or small ground antennas, seaboard ship systems such Phalanx Close In Weapon System (CIWS), aircraft GPS steerable antennas, and multiple spacecraft antenna systems.

The requirement for implementing an optimal control maneuver is just another form of implementing an arbitrary trajectory maneuver. The focus of this thesis was to implement a simple minimum energy maneuver based on modeling the system as two double integrators. The minimum energy trajectories are input as a position and velocity maneuver (describe in Chapter IV) and operate on motorized gimbals (joints) as previously mentioned.
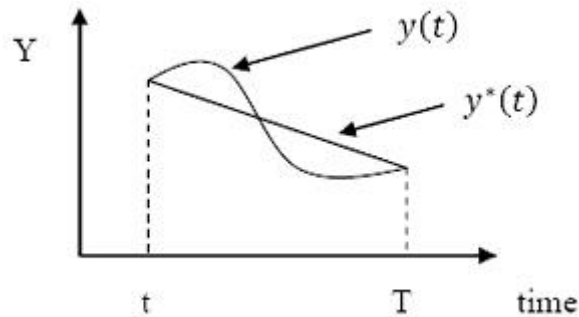
Figure 3.   Comparison of Optimal Path y(t) With Non-Optimal Path y*(t)

THIS PAGE INTENTIONALLY LEFT BLANK

III. TESTBED DESIGN AND INTEGRATION

A. INTRODUCTION

In this chapter, the design considerations and process of integrating and building the testbed are discussed. The process for designing parts and subsequent iterations that led to the completed testbed assembly are also discussed. Additionally, in this chapter, the motor choices are examined and the implementation of hardware used to provide the functionality of the testbed is described. Finally, the software chosen to operate the motor controllers is discussed as is the programming that was implemented provided versatility and agility required by design constraints outlined in Chapter II.

B. DESIGN CONSIDERATIONS

1. Design Iterations

The design iteration process can be a long difficult process if one is not prepared for design iterations and does not have a plan to make changes as necessary to attain a final product. When engineering design components are coupled, they often require multiple iterations; this is especially true in a large engineering project, when there is a convergence of many components or when many features are coupled [8]. Multiple iterations are the result of design changes and may be rooted from errors made when specifying tolerances and the clearances between parts. There is a chain reaction associated with multiple iterations; where a connection between two parts that are coupled may cause a shift in mass or reduce clearance needed on the completed assembly. Figure 4 shows the iterative design process loop for designing a final product. To reach a final part design, multiple iterations are needed to allow for reduced errors in clearances and tolerances. In this thesis, the design process began with paper drawings and continued into CAD modeling. The CAD program used was Solidworks® 2012. The author had undergraduate experience with Solidworks and using CAD, therefore taking paper ideas into CAD was not a difficult transition. The iterations were prototyped using rapid prototyping described in Chapter II.B. Several design iterations were made using 3D printing because of errors in the fit of parts, new ideas that were introduced during the

13

design process, and the ease of using a rapid prototyping system when designing multiple parts. Use of the iterative design process resulted in the final testbed shown in Figure 5.
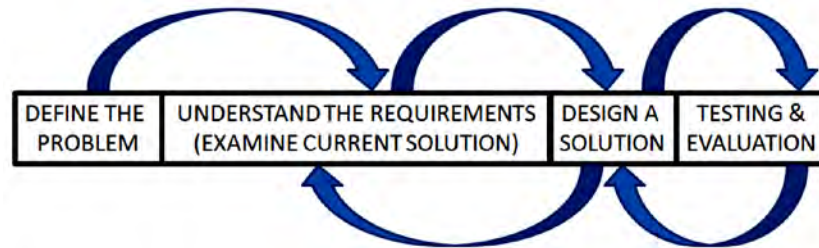
Figure 4.   Iterative Engineering Design Process (from [3])
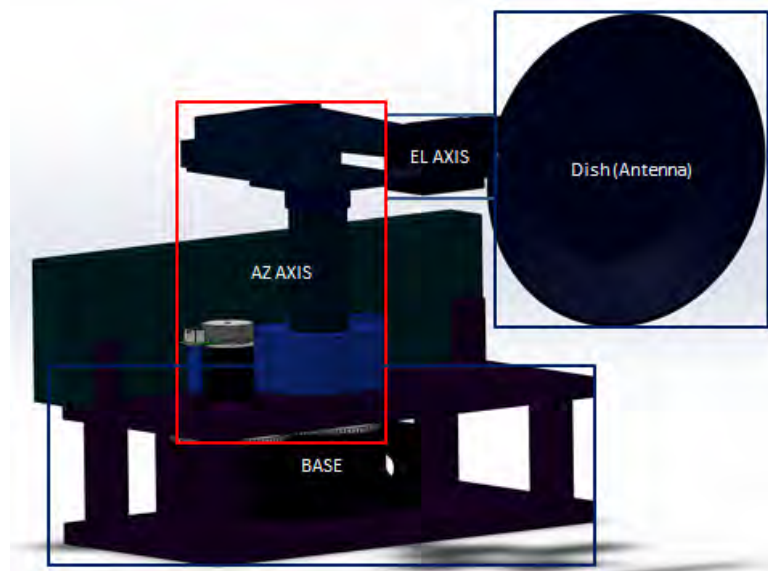
Figure 5.   Completed Antenna Slew Testbed

The physical system design requirements included the need to design, develop, and test a multiple axis gimbal to maneuver an antenna dish for both conventional and optimal slew maneuvers. The specific requirements were two axis gimbals (elevation and azimuth), minimum .01 rpm and maximum 50 rpm, +/- 360 degree motion on azimuth and +/- 30 degree on elevation. Additionally, the testbed had be designed as modular as possible to implement or mimic various antenna gimbal designs and accordingly enable scaling to implement different types of profile maneuvers.

2. Rapid Prototyping

Rapid prototyping described in Chapter II, was a method for quickly changing design to implement in the next iteration. Figure 6 shows the design iterations per part needed and their associated mates that converged to a final assembly.
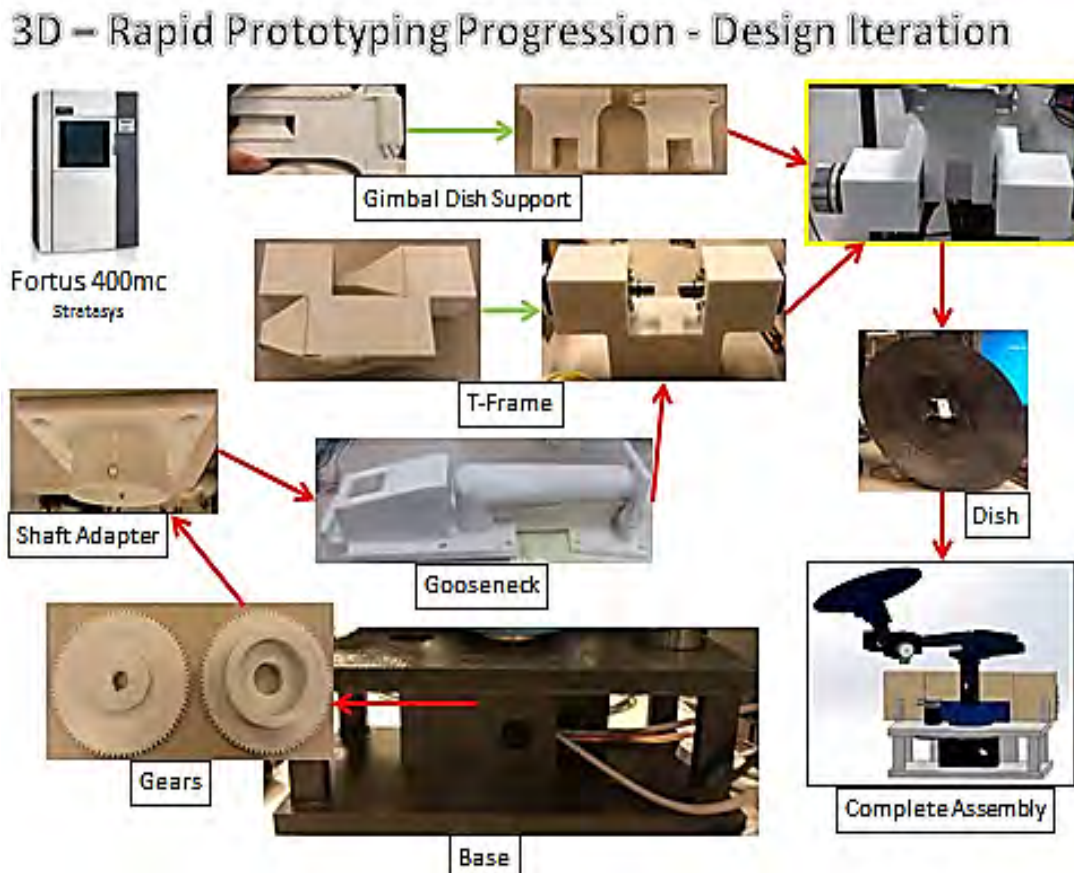
Figure 6.   Rapid Prototyping Progression for Testbed Development

The Fortus 400mc was limited to 406 x 356 x 406 mm build dimensions. Therefore, a lot of consideration must be taken before designing parts. As stated, Solidworks was used to import the .STL files into the Fortus for printing. The NPS rapid prototyping wiki states that the:

> approximate cost (part material alone) is about $4.50 per cubic inch. Canisters of material and support come in 92 cubic inch canisters and cost between about $400 and $450 each, depending on the type of material. Note that some waste is involved with calibration parts and in the normal

operation of the machine. Materials supported are the white polycarbonate (PC) (P/N: 310-20100 [9]) and this was used for all parts. [5]

C.   ANTENNA MECHANISM

1.   Base

The base assembly was composed of the base, the gear support block, and two gears. The base was the support structure for the azimuth gimbal and also supports the entire testbed.

The gear support block holds the gears as they rotate and houses the electrical cables that are routed through the PVC support shaft. The cables are then routed through the gear support block holes. The block had to be sanded and lightly greased to provide minimal friction for the gears. This block can be replaced in future prototypes with roller bearings to better support each gear and further reduce friction.

The gears are two separate gears designed with a gear-pinion ratio of 1 to 1. The motor output gear connects to the drive motor output gear keyway. Reference [10] states that tooth-to-tooth composite backlash tolerance should be in the range of .0001 to .0007 inches between gears, and by design the testbed gears limit backlash (the gears were designed within the range for backlash tolerance) and provide smooth translation between gear (motor output gear) and pinion (shaft connection gear) meshes. Figure 7 is a photo of both manufactured gears. Several design iterations were conducted to size and resize the gears for clearance and tolerance purposes (to meet backlash standards). The base houses the gears and gear support block as shown in Figure 8 and Figure 9. The shaft connection gear (pinion) has the PVC shaft inserted in the insert (extruded shaft) and connected by set screws as shown in Figure 8. The set screws translate the force from motor to gears to shaft, thus creating an azimuth gimbal.
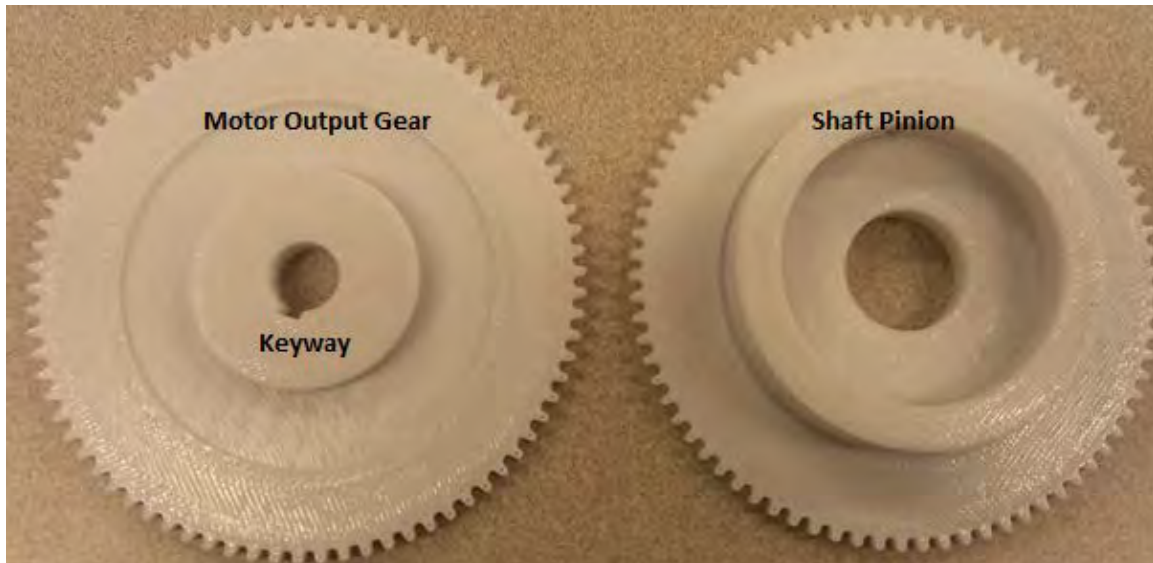
Figure 7.   3-D Printed Gear and Pinion
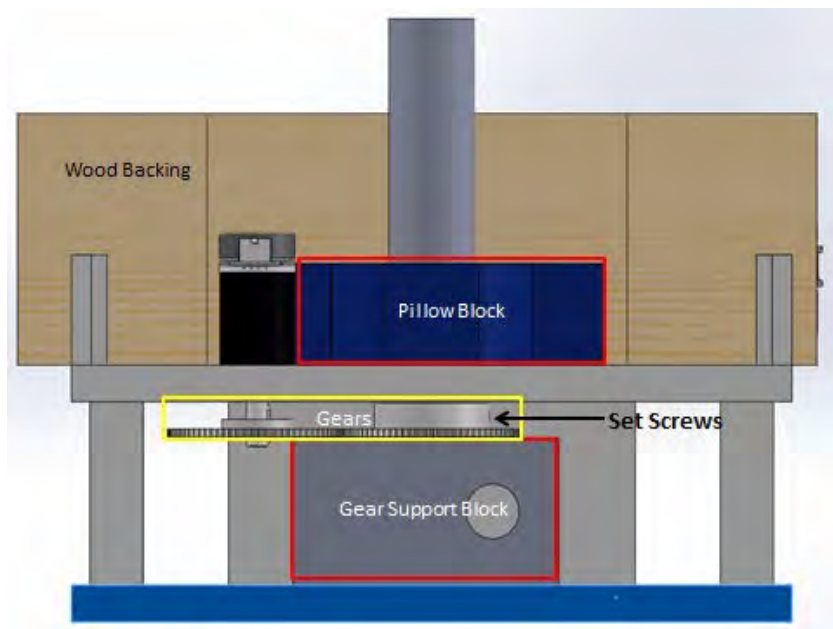
Figure 8.   CAD Model of Base Assembly
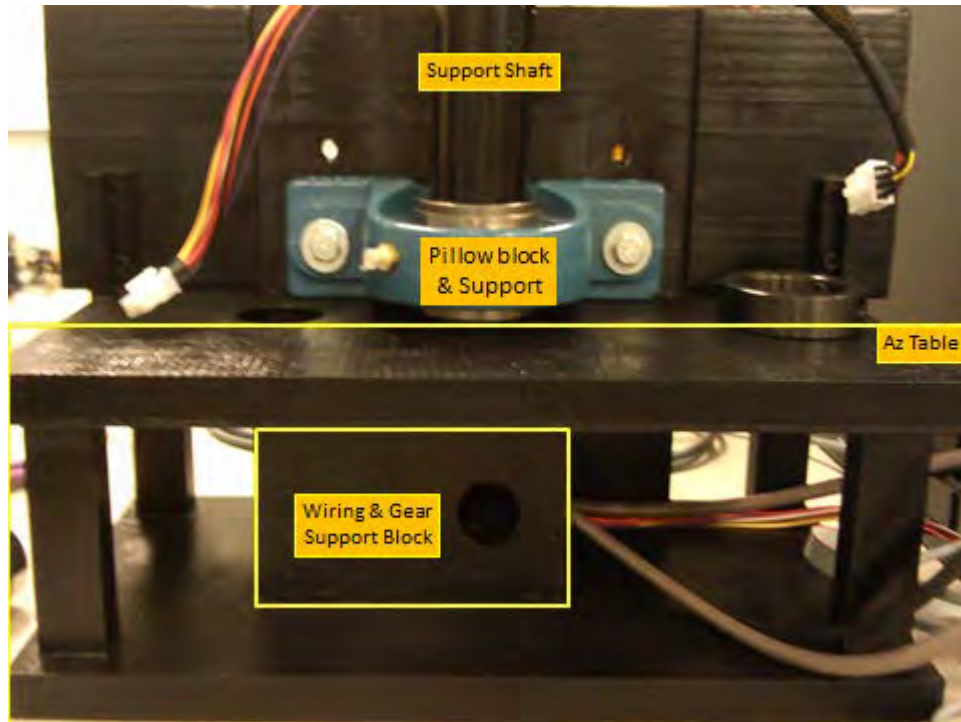
Figure 9.　Final Base Assembly

2.　Support Shaft

The support shaft assembly was comprised of the wood block, pillow block (joint bearing), PVC pipe, and gooseneck base. The wood block was screwed to the base and bolted to the pillow block. The wood used was spruce and the dimensions are somewhat arbitrary. Any rigid structure can be used to support the pillow block.

The PVC shaft supports the elevation gimbal. The PVC shaft was connected to the shaft gear and the gooseneck base and held up by the pillow block. Figure 10 shows a pillow block (model AK204). The pillow block was used to support the shaft and the mass of the elevation gimbal. The pillow block has a bearing to provide smooth rotation of the PVC shaft. The pillow block was used for maintaining a mounting surface parallel to the pin axis [10].

Figure 10.   AK204 Pillow Block Bearing

Figure 11 shows the gooseneck support plate (GSP). The GSP connects the shaft to the gooseneck (described in Chapter III A3). It is held in place on the gooseneck by four bolts and translates the azimuth rotation with set screws into the PVC shaft. Several design iterations were made so that the set screw holes would not shear when rotating about the azimuth joint. The support shaft assembly attached to the base is shown in Figure 12.

Figure 11.   Gooseneck Support Plate (GSP)
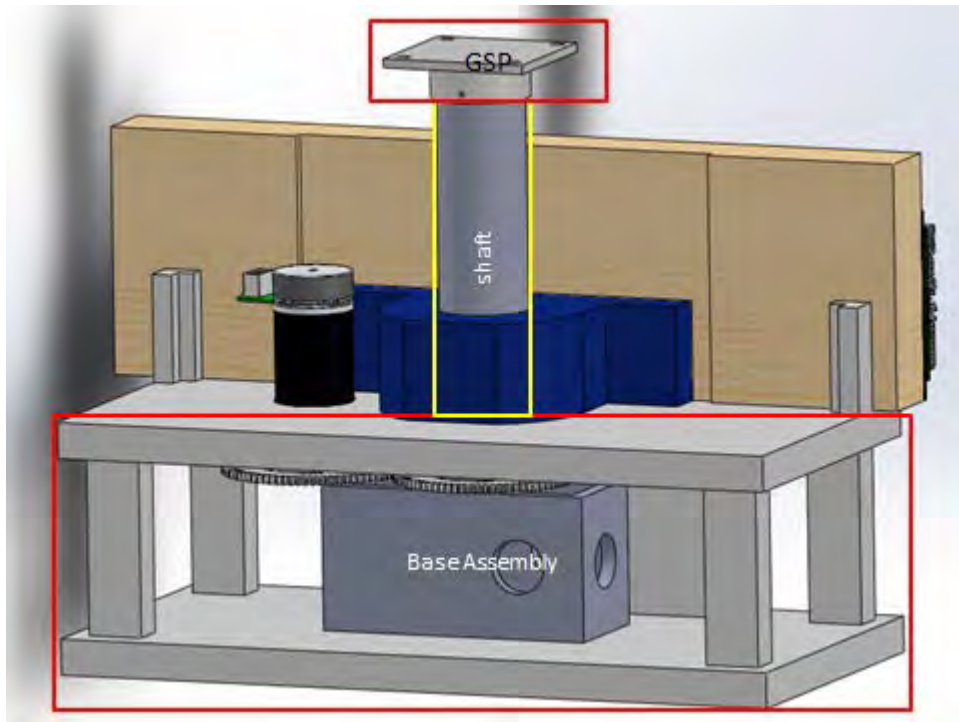
Figure 12.   Support Shaft Assembly Mounted to the Base

3.   Gooseneck and Counter Weighting

The gooseneck connects to the PVC shaft above the GSP and supports the elevation gimbal by connecting to the T-frame. The design was thought up by the author to provide clearance for the dish and elevation gimbal while maneuvering as to not impede on the base structure. The elevation gimbal causes a moment at the end of the gooseneck; so a counterweight can be used to zero (balance) the moment with respect to the center of the PVC shaft. The design therefore incorporates a hook to hold counterweights to offset the mass of the elevation gimbal and dish (the free body diagram is shown in Figure 13). Additionally, there was a countersink integrated into the gooseneck to hold mass to counterbalance the elevation gimbal mass. Figure 14 shows the gooseneck attached atop of the previous assemblies. Chapter VI discusses alternative designs that can be implemented in the future that reduce the need for a counterweight system.
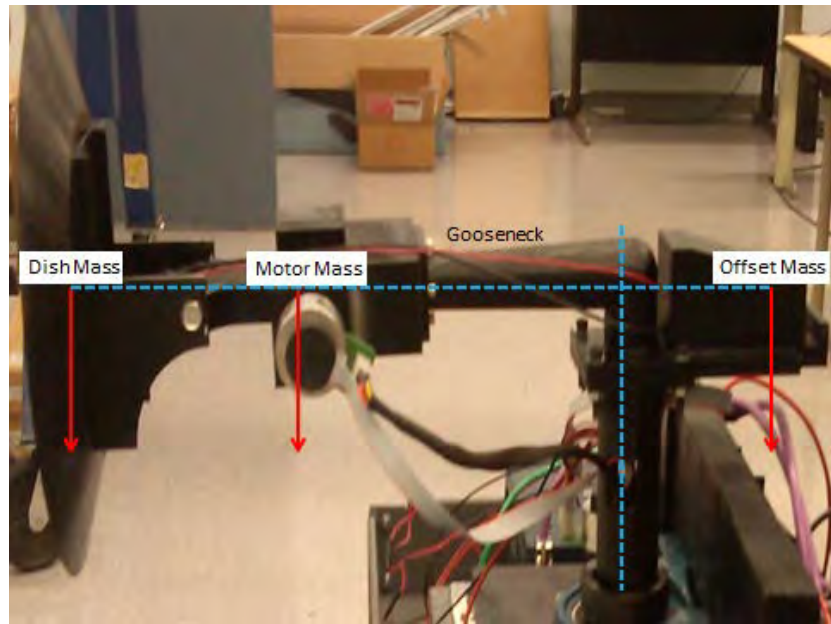
Figure 13.   Free Body Diagram on Gooseneck and Elevation Gimbal Assembly
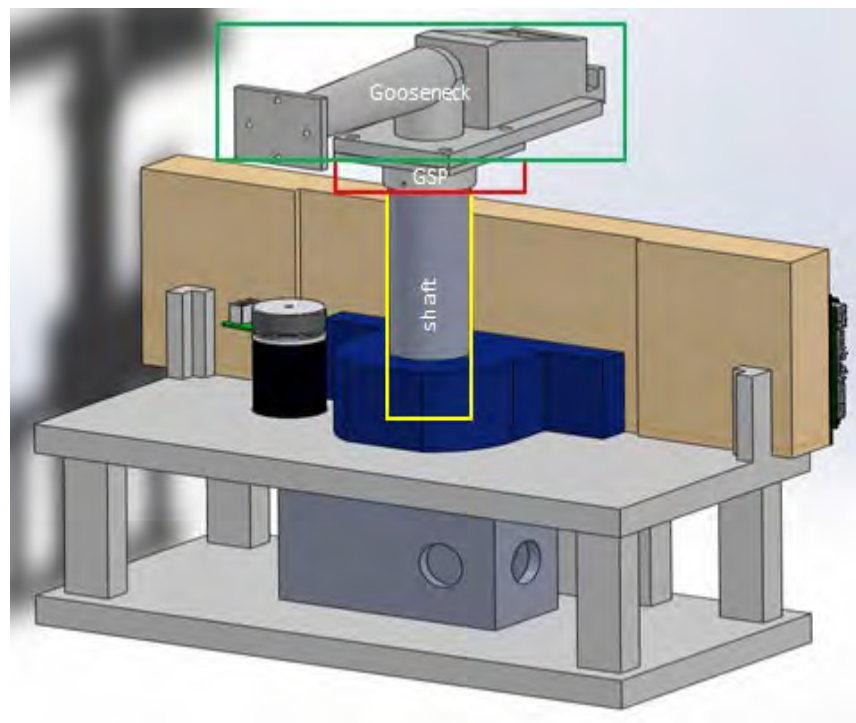
Figure 14.   CAD Model of Gooseneck Assembly Integrated with the Support Shaft

4. T-Frame, Antenna Gimbal and Dummy Shaft

The elevation gimbal assembly consists of the T-frame, the antenna gimbal, and a dummy shaft. All parts were manufactured using 3D printing with the exception of the drive motor used for the elevation gimbal. Figure 15 shows how the T-frame bolts to the gooseneck. Figure 16 shows a transparent view of the T-frame to illustrate the dummy shaft and motor mounting.
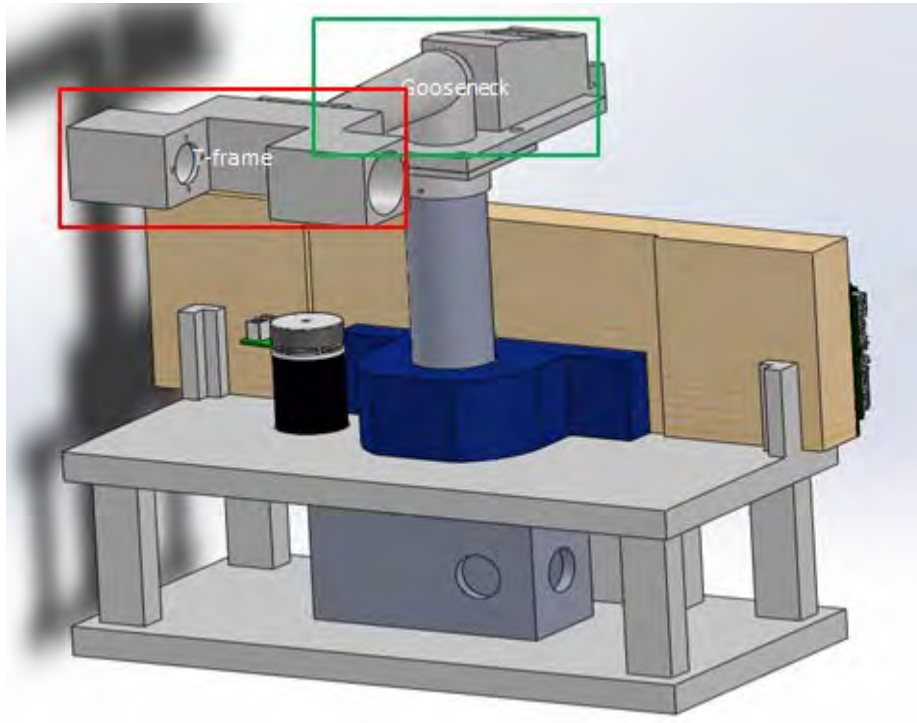
Figure 15. T-Frame Assembly

Figure 17 shows how the motor is bolted to the inside bore holes of the T-frame on the gear train flange and the completed elevation gimbal assembly.
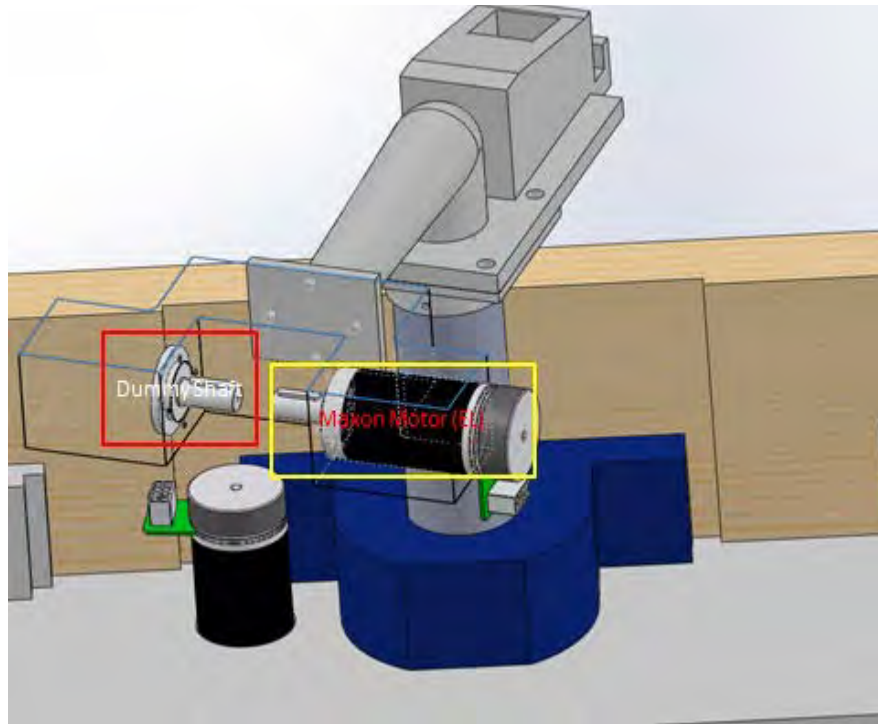
Figure 16.   T-Frame Assembly (Transparent View)
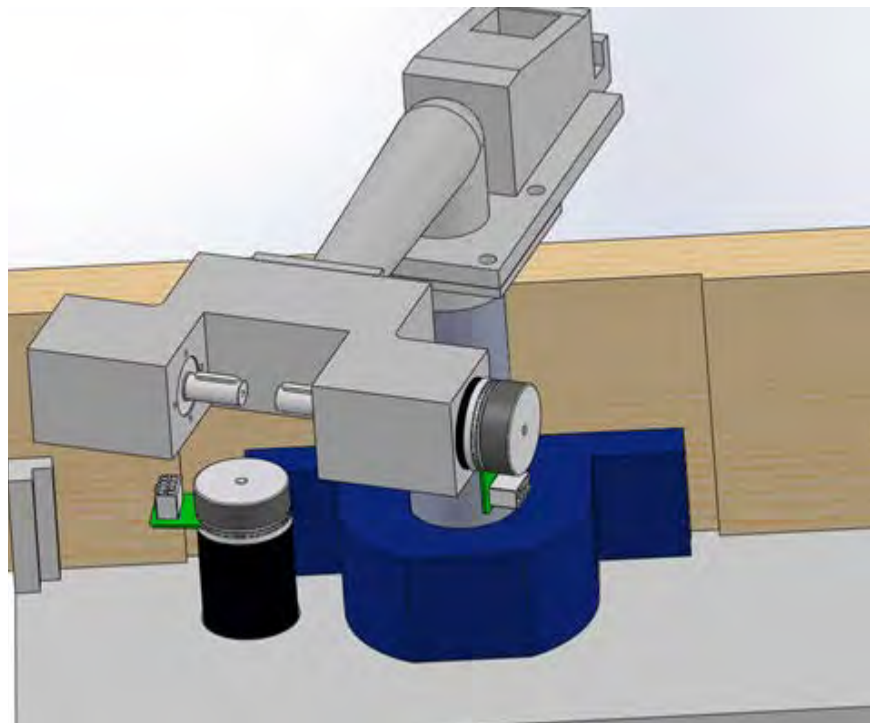
Figure 17.   Complete Elevation Gimbal Assembly

Figure 18 shows the gimbal support piece. The gimbal support piece is held by the keyway on the gear train output (of the elevation motor) and the dummy shaft with equivalent dimensions of gear train keyway. The dummy shaft allows for even support of the mass of the gimbal support piece in-between the inside section of the T-frame. The gimbal support piece translates the motion of the motor-gear train output as an elevation gimbal angle used to elevate the dish. The piece connects to the dish by bolting onto tapped holes.
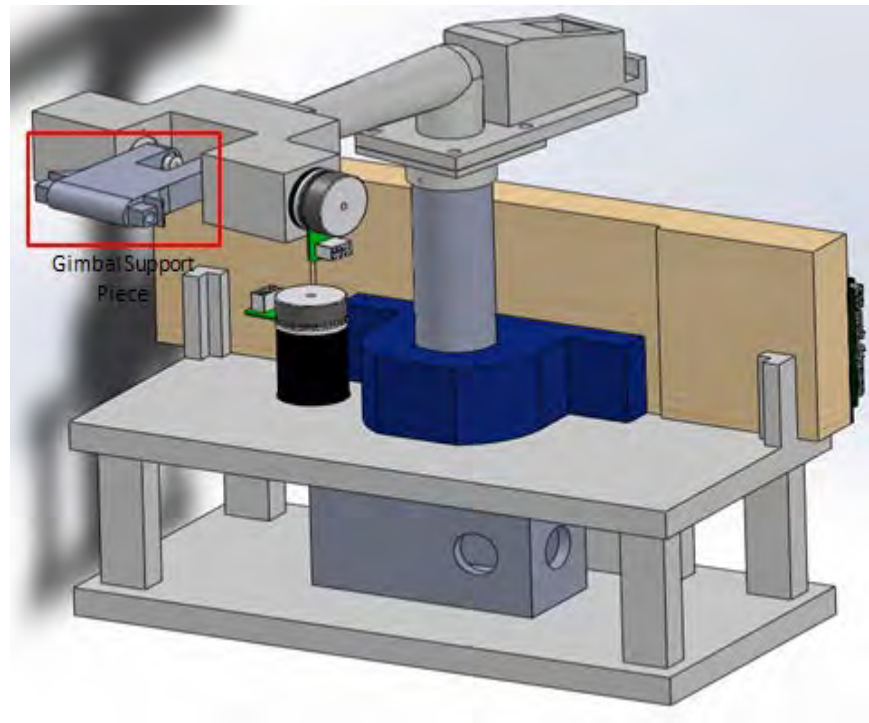
Figure 18.   Elevation Assembly with Gimbal Support Piece

5.   Antenna Dish

Figure 19 shows the antenna dish, also printed in plastic. The dish connects to the gimbal support piece by bolts in the stem extending from the dish. The dish supports a small 5v laser mounted in the center (not shown in Figures). The laser was for demonstration purposes to project the maneuver path of the gimbals in the laboratory during trajectory experiments.
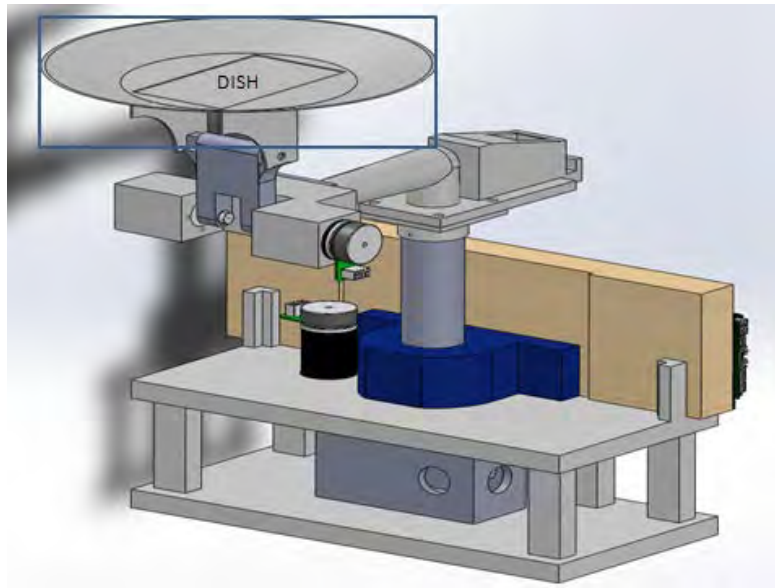
Figure 19.   Antenna Dish and Elevation Gimbal Assembly

6.   Complete Assembly

Figure 20 to Figure 22 show the complete testbed assembly in different views.
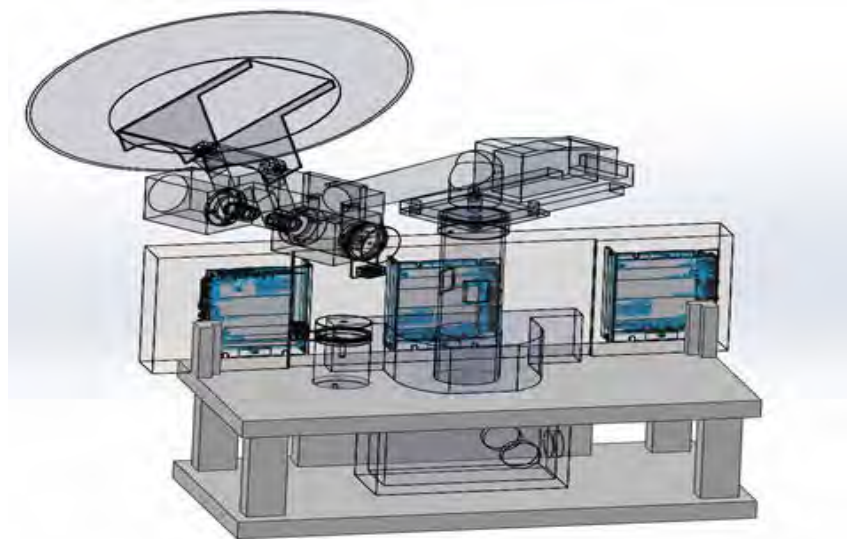
Figure 20.   Complete Antenna Testbed Assembly (Transparent View)
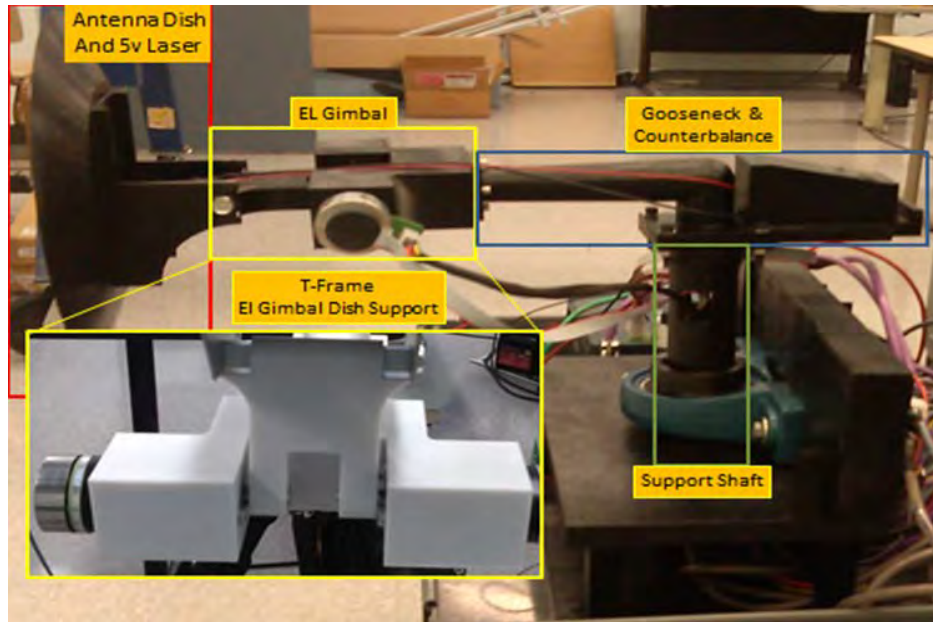
Figure 21.   Complete Gooseneck and Elevation Assembly
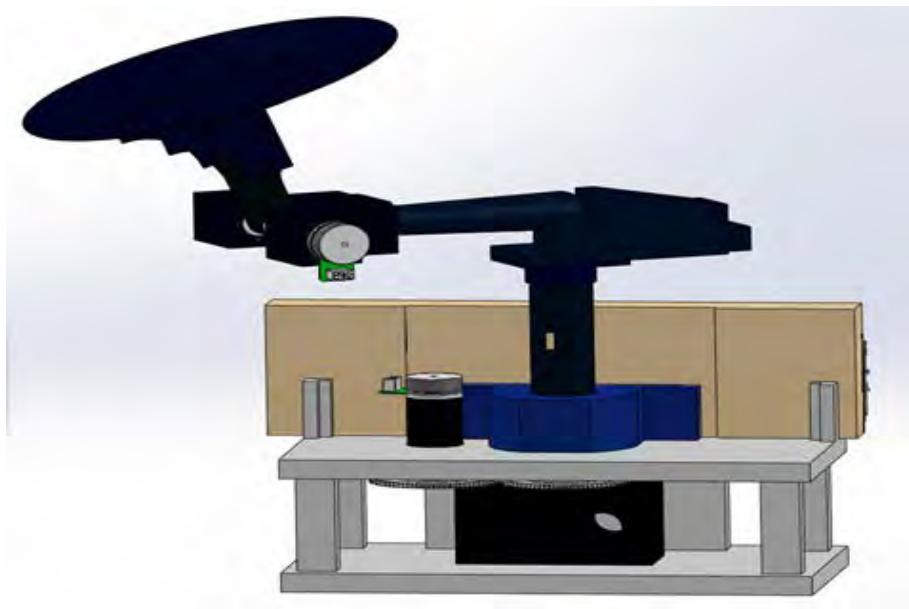
Figure 22.   Complete Antenna Testbed Assembly

D.   GIMBAL MOTORS

1.   Motor Selection and Control Laws and Gain Tuning

COTS motors are typically either brushed or brushless DC motors. Ackman's thesis has a comparison of the two types and characteristics for both [3]. It was concluded

that brushless DC (BLDC) motors allowed for an easy integration into the overall design, are reliable, provide high torque-to-inertia values, and require little maintenance. This thesis utilized the Maxon EC Flat motors based on the recommendations of reference [3] and the assessments of various BLDC motor vendors. Ackman also concludes, "not only does the Maxon motor meet all the required parameters, but is readily in stock for future purchases and is considerably smaller than the other motor choices" [3]. The author encourages the reader refer to reference [11] to understand the fundamentals of BLDC theory and operation. Figure 23 shows the AZ and EL axis requiring the BLDC motors.

Figure 23.   Gimbal Axis Rotation and Motor Locations

In addition to the motors, themselves, a gear train can be attached onto the motor if specified. The selected gear trains (described in detail in Section E.1.e) are attached to the output of the motor and provide a 113 to 1 reduction. The gears are precision spur and planetary gearheads. The motor pinion is the input gearwheel for the first stage and is rigidly affixed to the motor shaft [12]. The gear train was selected for its high reduction rate, low mass, short gearhead length, and large axial load capability to support the mass

(increased torque) of the gimbal support piece and dish. Figure 24 shows both the gear train and EC flat motor. The vendor also provides the EPOS2 motor controller for operating the EC motors.

Figure 24.   Maxon Motors Gear Train and EC Flat Motor (shown left to right) (from [12])

The EPOS2 motor controller was connected to the PC using RS232 connector or a USB and was programmed through the EPOS Studio 2.0 software. The software provided the capability for automatic gain tuning and standard motion control such as position, homing, profile velocity, position, profile velocity and current modes [13]. The motor gains were tuned using the EPOS studio auto regulation tuning with the 113-reduction gear train and 3-channel hall sensors attached. The auto regulation tuning allows for three essential regulation structures to be tuned: the current control loop, the position control loop, and the velocity control loop [14]. Figure 25 shows the controller architecture. The block diagram for current regulation, velocity regulation and position regulation structures are shown in Figure 26, Figure 27 and Figure 28, respectively. As seen, the motor controller uses a closed loop control structure to operate the motor. Typical automatic-tune results for current, velocity, and position are shown in Figure 29. Table 1 shows the gains obtained after tuning. The units are given in EPOS2 parameter units. Conversion factors for SI units are available in reference [12]. Expert tuning mode can be used to further tune gains for better performance and optimal motor operability. When the system operates in position control mode, as was done to implement the experimental maneuvers discussed later, the EPOS2 motor controllers operate using the current and position closed loops shown in Figure 26 and Figure 28.

28
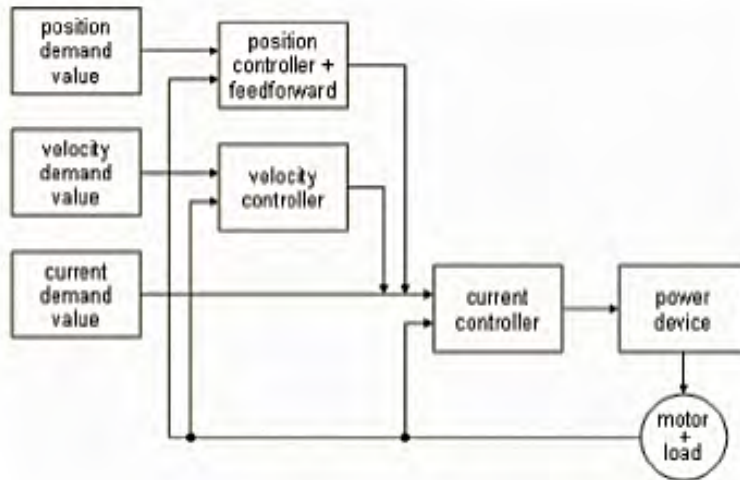
Figure 25.   Maxon Controller Command Diagram (from [14])
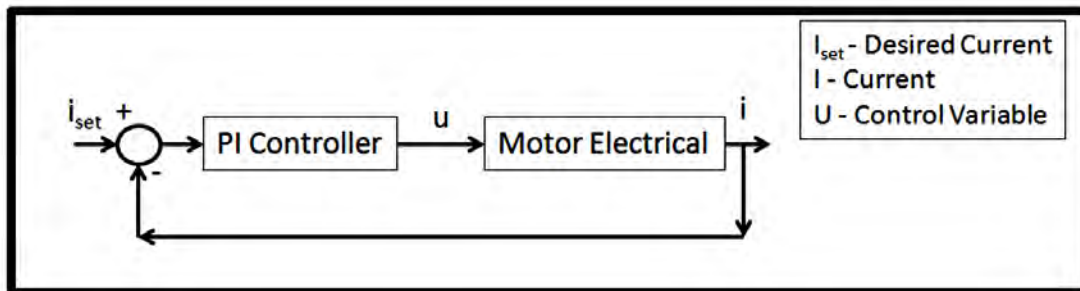
Figure 26.   Maxon EPOS2 Current Control Loop (from [14])
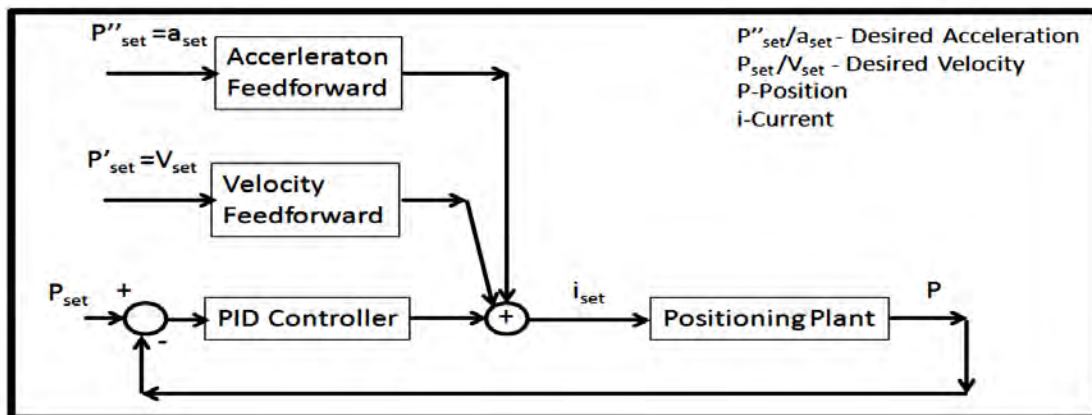
Figure 27.   Maxon EPOS2 Velocity Control Loop (from [14])
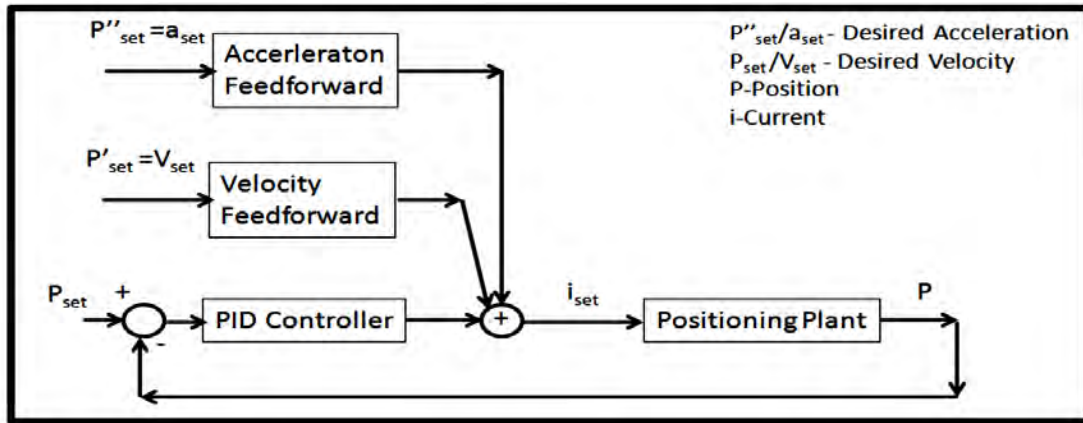
Figure 28.   Maxon EPOS2 Position Control Loop (from [14])
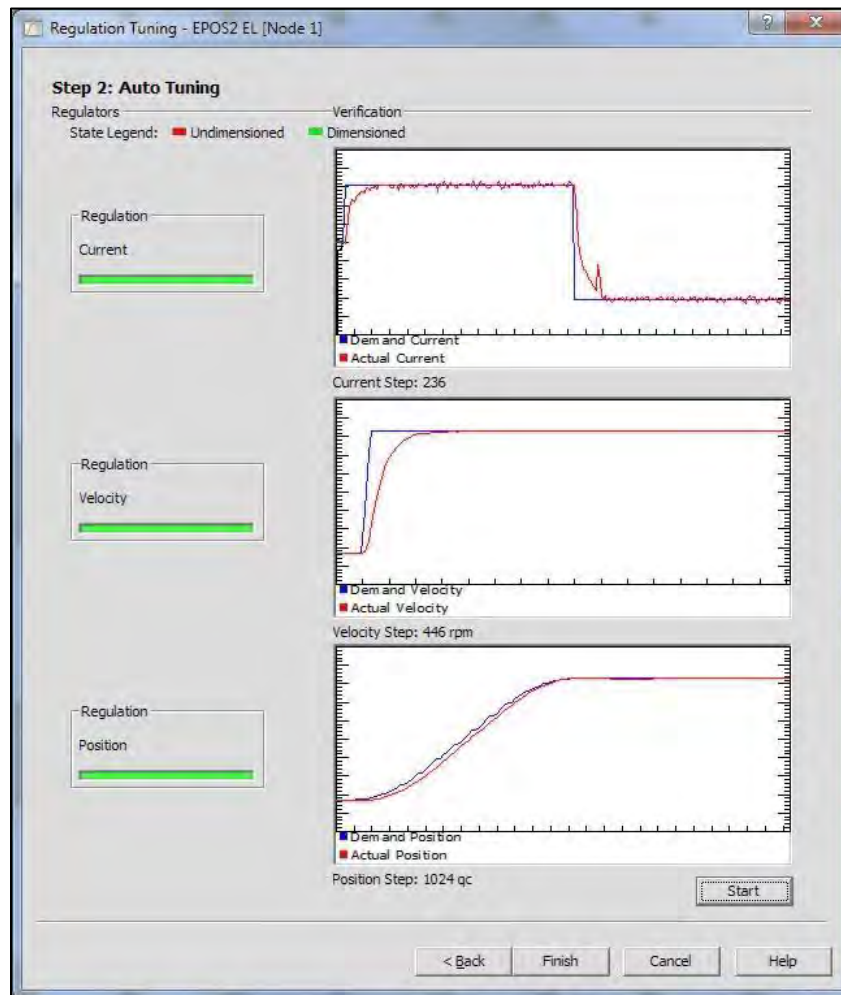
Figure 29.   Controller Gain Tuning Results

Tuning Parameters			
Gains	Current	Velocity	Position
P	510	2263	404
I	89	269	1027
D	-	-	849
Velocity FF* Factor	-	0	0
Acceleration FF* Factor	-	378	378
*FF: Feed Forward			

Table 1.   Final Control Law Gains For AZ and EL Gimbals

a.   *Axis Architecture Setup*

The elevation (EL) and azimuth (AZ) gimbals represent a two degrees-of-freedom (2-DOF) system. The EL axis was limited by design to +/- 90degrees and the AZ has no limit in rotation. Figure 30 depicts a ground system AZ axis and EL antenna system.
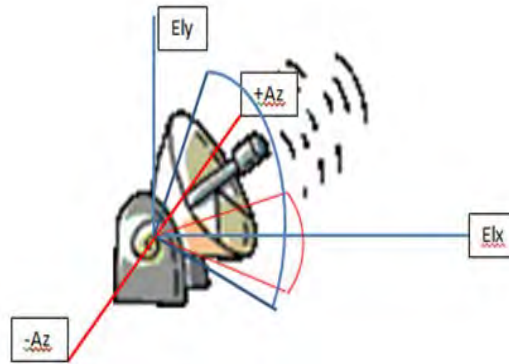
Figure 30.   AZ and EL Gimbal Rotation Illustration

Figure 31 shows the hardware realization of a single axis setup, while Figure 32 shows a dual axis (AZ and EL) setup. a single axis architecture was needed for early testing of a single EPOS motor controller and motor. The dual axis setup was used later and utilizes two EPOS motor controllers and two motors (dual or multiple axis system) using the CANopen system (described in Section C.2). The final system used on the testbed was the dual axis setup. The software and hardware for a dual axis are described later in the next section.

Figure 31.   Hardware Needed for a Single Axis Setup

Figure 32.   Hardware Needed for a Dual Axis Setup

E.   INTEGRATION

This section describes the integration of all the components needed to assemble and instrument the testbed. The final design combines COTS hardware, 3D printed components, electronics, software (included with hardware), and in-house manufactured parts and fasteners. This section steps through all the components that make up the final testbed (prototype) and how those components and subcomponents are assembled to complete a working and moving testbed. The bill of materials is given in Table 2 and lists all final hardware used in the final design iteratio. The bill of materials includes COTS equipment, 3D printed parts, wiring, and student manufactured miscellaneous equipment. The testbed was intended to last throughout several prototype design iterations for future theses or testing. The bill of materials lists the materials the components are composed of, for example Polycarbonate plastic (PC), which was described in Section A.2. The Maxon motors are comprised of several materials, but labeled ceramic because of the motor casing coating. Polyvinyl chloride (PVC) was used to build the support shaft. The pillow block manufactured by many companies is cast iron; it was supported by spruce wood platform (2x6 inch) with purchased fasteners. The laser was a circuit board cased in a copper tube. The "Comp" symbol represents a controller or computer that is primarily circuitry. CAB is a shortword for the cables that were manufactured in-house by the author.

Bill of Materials					
List #	Part	Company	Part #	Quantity	Material*
1	Base	NPS	1	1	PC
2	Wiring Box	NPS	2	1	PC
3	Az Gear	NPS	3	1	PC
4	Shaft Gear	NPS	4	1	PC
5	AZ Maxon MEG	Maxon	M131076	1	Ceramic
6	Shaft	N/A	6	1	PVC
7	Pillow Block	Any Bearing	AK204	1	Cast Iron
8	Wood Support	N/A	8	1	Cedar
9	Shaft Plate	NPS	9	1	PC
10	Gooseneck	NPS	10	1	PC
11	T-Frame	NPS	11	1	PC
12	Gimbal Neck	NPS	12	1	PC
13	EL Maxon MEG	Maxon	M131076	2	Ceramic
14	Dummy Shaft	NPS	14	1	PC
15	Dish	NPS	15	1	PC
16	5v Laser	Any Electonics	5v Laser	1	Copper
17	EL Maxon EPOS2	Maxon	367676	1	Comp
18	AZ Maxon EPOS2	Maxon	367676	1	Comp
19	cRIO NI9024	NI	781174-01	1	Comp
20	NI9113	NI	780917-01	1	Comp
21	NI9853	NI	779429-01	1	Comp
22	Power Supply	EXTECH	382213	1	Comp
23	PC	DELL	Optiplex790	1	Comp
24	RS232-EPOS Cable	Maxon	275900	1	CAB
25	Serial-CAN Cable	Maxon	275908	1	CAB
26	CAN-CAN Cable	Maxon	275926	1	CAB
27	Hall-Motor Sensor Cable	NPS	27	2	CAB
28	Encoder Cable	Maxon	275934	2	CAB
29	EPOS Power Cable	Maxon	275829	2	CAB
30	Misc Hardware**	NPS	30	-	-

Table 2. Bill of Materials for Antenna Testbed

1. Hardware

The hardware used on the testbed was chosen based on the requirements of having a real-time system that could be purchased as commercial-off-the-shelf (COTS) parts or manufactured in the lab throughout the design process. Custom hardware was also purchased to meet the required tolerance requirements (e.g., motor speeds) to more

closely match the actual systems the testbed is meant to simulate or mimic. The conclusions (Chapter VI) will discuss issues the selected hardware caused and the engineering used to solve those problems to have a working testbed. The hardware, as with all designs, went through the rigorous market research to compare and eventually pick the best equipment and a reasonable price (best value choice) to construct the testbed.

a.   Power Supply

The power supply used in the testbed is an Extech 382213 DC power supply regulator with digital display. It is used to supply approximately 22v to the EPOS2 motor control boxes and the NI cRIO-9024 (described in later sections) as well as to provide a continuous 5v to the laser as shown in Figure 33.
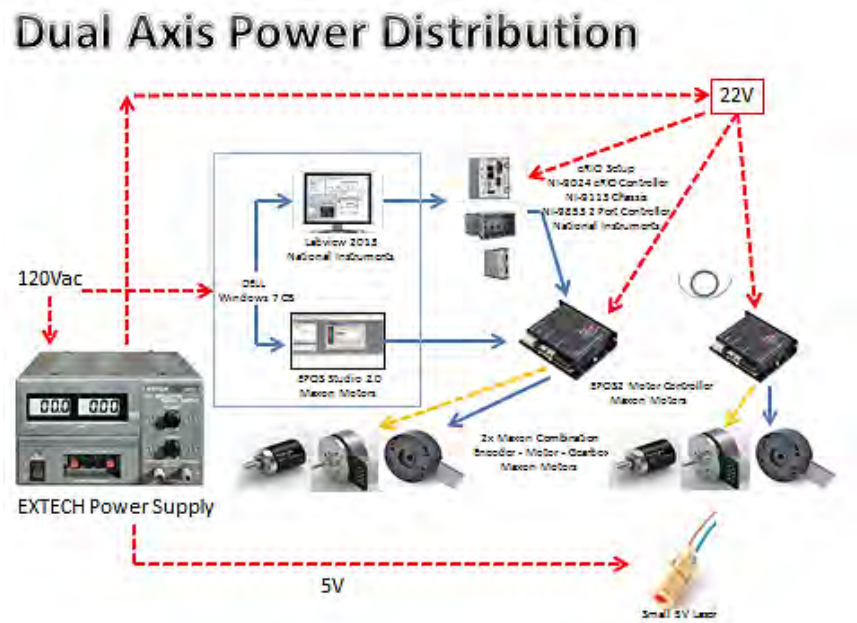
Figure 33.   Dual Axis Power Distribution Setup

b.   PC

A personal computer (PC) was used for: a) communications with the EPOS 2 controllers and b) communications with the NI cRIO (compact RIO) as shown in

Figure 34. The PC used was a DELL OPTIPLEX 790, with Windows 7 OS SP-1 PC, Intel COREi5 at 3.1GHz and 4GB RAM. Any PC that supports the software requirements of EPOS studio 2.0 and NI LabVIEW 2013 software would meet requirements to operate the testbed.

c.   NI Hardware (cRIO, Chassis, Controllers)

The NI equipment was recommended by Maxon Motors when requesting a system that would communicate with the EPOS motor controllers with real time ability. The NI equipment supports the CANopen architecture. CANopen functionality and operation is explained in Section C.2.b. CANopen provides a means for enabling multiple motors to run simultaneously and/or in tandem (shared axis, opposite polarity). After market research with CANopen systems, the NI cRIO system was chosen, purchased and implemented based on the feasibility, availability and legacy software drivers for EPOS2 motor controllers.

The NI cRIO system (see Figure 34) encompasses three subcomponent systems: 1) NI cRIO-9024 controller. The NI cRIO-9024 is a real-time controller with 800 MHz, 512 MB DRAM, 4 GB storage. 2) NI-9113 is a 4-Slot, Virtex-5 LX50 CompactRIO Reconfigurable Chassis that connects to the NI cRIO-9024 and holds the NI 9853. The NI-9113 has a Xilinx Virtex-5 reconfigurable I/O (RIO) FPGA core and ability to automatically synthesize custom control and signal processing circuitry using LabVIEW; 3) NI-9853 is a 2-port, high-speed CAN module with a standard DE9M (DB9) male connector for each port, Philips SJA1000 CAN controller and Philips TJA1041 CAN transceiver [15]. Figure 34 shows the three devices. The NI-9853 communicates to the EPOS2 motor controller boards via a serial-CAN cable (shown in Figure 35). Table 3 and Table 4 show the cable pin connections required for the Serial-CAN cable. Figure 36 shows the NI cRIO system assembly as constructed in the lab.
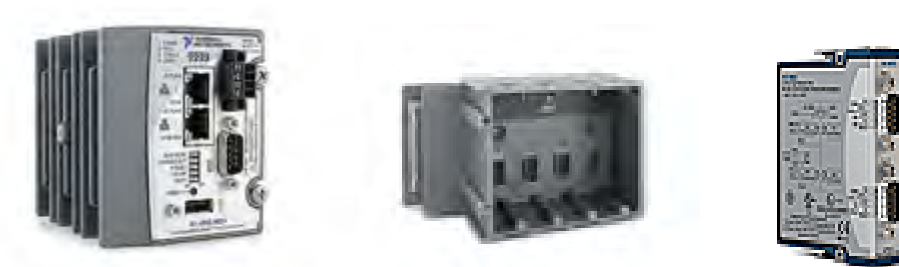
Figure 34. NI-9024, NI-9113, NI-9853 (Shown Left to Right)

Figure 35. Serial-CAN Cable

Wire	Head A Pin	Head B Pin	Twisted Pair	Signal	Description
yellow	1	7	1	CAN high	CAN high bus line
green	2	2		CAN low	CAN low bus line
brown	3	3	–	CAN GND	CAN ground
black	4	5	–	CAN shield	Cable shield

Remark:
pin assignment according to CiA DS102-2

Table 3.   Pin Connection Assignments for CAN (from [15])

Connector	Pin	Signal
	1	No Connection (NC)
	2	CAN_L
	3	COM
	4	NC
	5	SHLD
	6	COM
	7	CAN_H
	8	NC
	9	NC

Table 4.   Pin Connection Assignments for CAN (from [15])
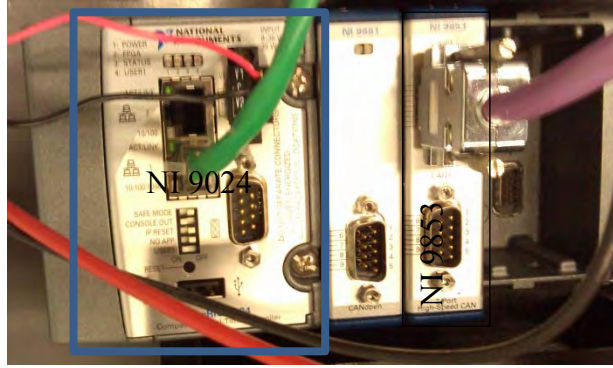
Figure 36.   NI System Assembly in the lab (NI-9024, NI-9113, NI-9853)

d.   EPOS2 and EPOS2-P

The AZ and EL motors are operated using a Maxon EPOS2 (Easy to use POSitioning) 24/5 position/velocity controller shown in Figure 37.

Figure 37.   EPOS2 Motor Controller

The EPOS2 24/5 controller is a full digital, smart motion, controller that allows for the user to communicate and control EPOS enabled devices. As previously mentioned, the motor controller was connected to a computer using RS232 connector or USB and was programed through the EPOS Studio software. This provided the capability for automatic gain tuning and standard motion control modes such as position, homing, profile velocity, position, profile velocity and current control [14]. Figure 38 shows the minimal cable wiring needed for the EPOS2 with motor and encoder.
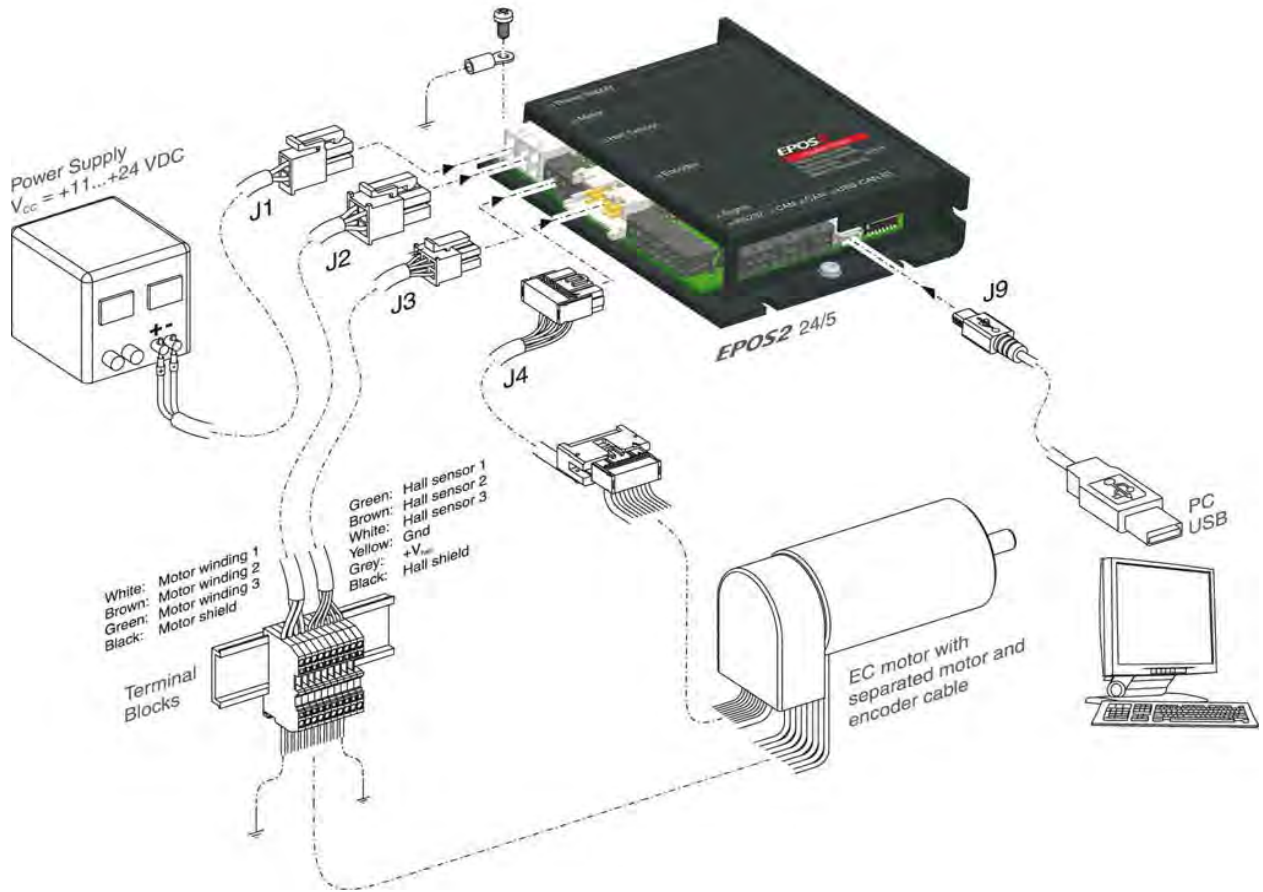
Figure 38.   Wiring Requirements for EPOS2 Motor Controller (from [16])

The EPOS2 provides the ability to communicate with up to 15 daisy-chained EPOS2 controllers over the CAN bus. Figure 39 shows how the master-slave CANopen architecture is established. The EPOS2 was pre-programmed using the EPOS 2.0 studio and then calibrated using the NI LabVIEW software. Both software support CAN-communications, however the EPOS studio uses USB or RS232. LabVIEW uses CAN-Serial cable communications because it is required for the hardware to enable real-time communications. Figure 40 and Figure 41 depict how the EPOS2 controllers were installed on the base of the testbed and how they were accounted for in the CAD drawings.
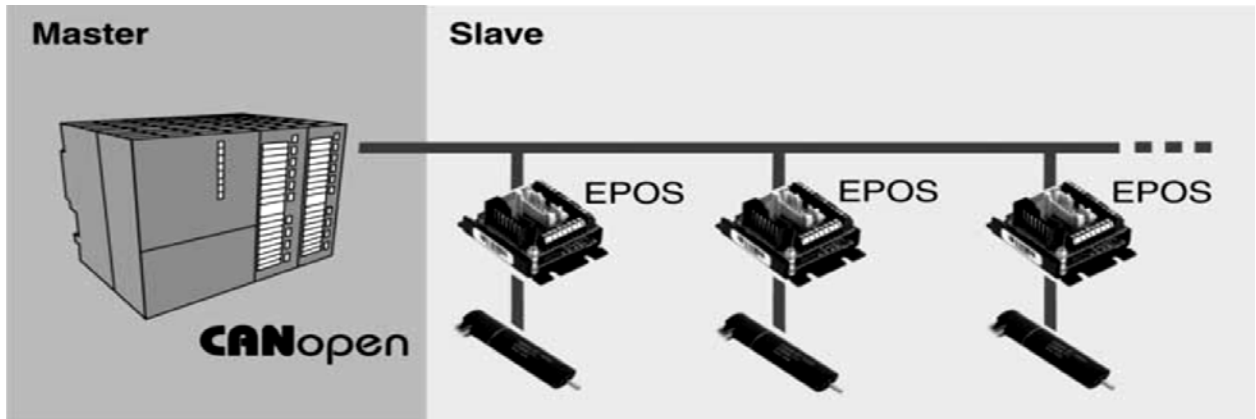
Figure 39.   Master-Slave Setup for EPOS2 (from [14])
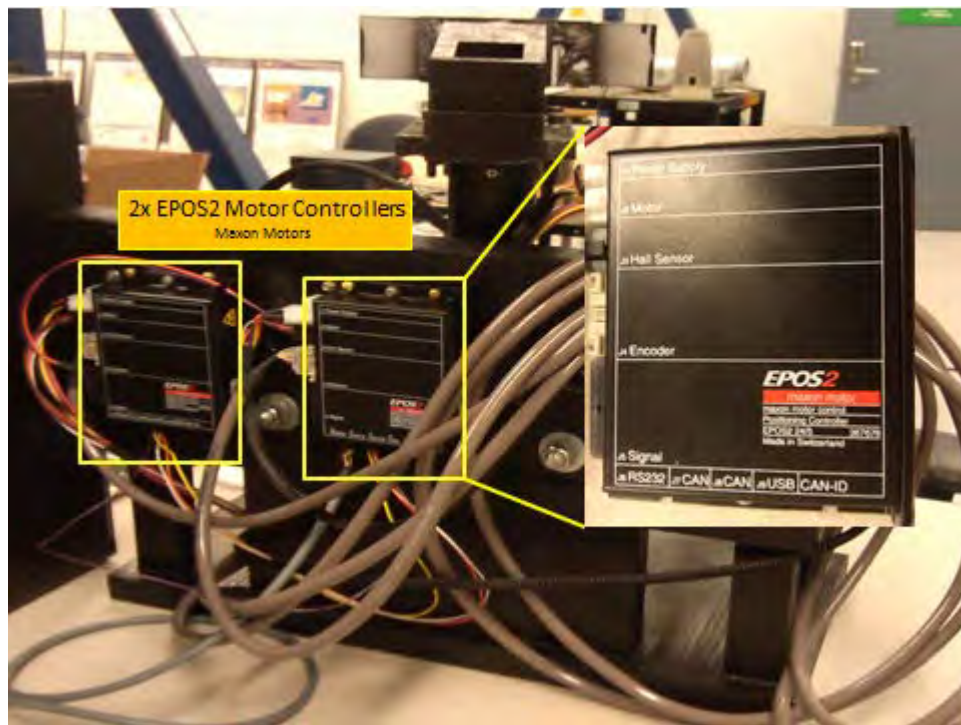
Figure 40.   EPOS2 Assemblies on Testbed

Figure 41.   CAD Model of EPOS2 Assemblies

e.   *Motors and Gear Reducers (Calibration and Setup)*

Motor theory and the setup for the Maxon motors are described or referenced in Section D.1. As mentioned previously, the motors used are the Maxon EC 45 flat motor with 113:1 reduction gear sets and a built-in encoder. Many of the preliminary tests were conducted with Maxon EC 45 Flat motors with hall sensors only in order to understand basic wiring and setup. Encoders were ordered after it was determined that a "smoother system" was needed for gimbal operation. Figure 42 shows the encoder (225787), motor (251601) and gear train (203126) purchased from Maxon Motors. Details and dimensional drawings are available on the Maxon Motor website [12] and in Maxon Motors catalogs [13].

Figure 42.   Maxon Motor Assembly—Gear Train, Motor, Encoder (Shown Left to Right)

f.   Wiring Harnesses and Communications

The testbed utilized Ethernet (TCP/IP), USB, RS232 serial, Maxon Serial-CAN cables, motor and encoder cables, and CAN-CAN cables. Figure 43 shows a single axis communications setup for the testbed. The single axis setup was initially used to test equipment prior to establishing a dual axis system.
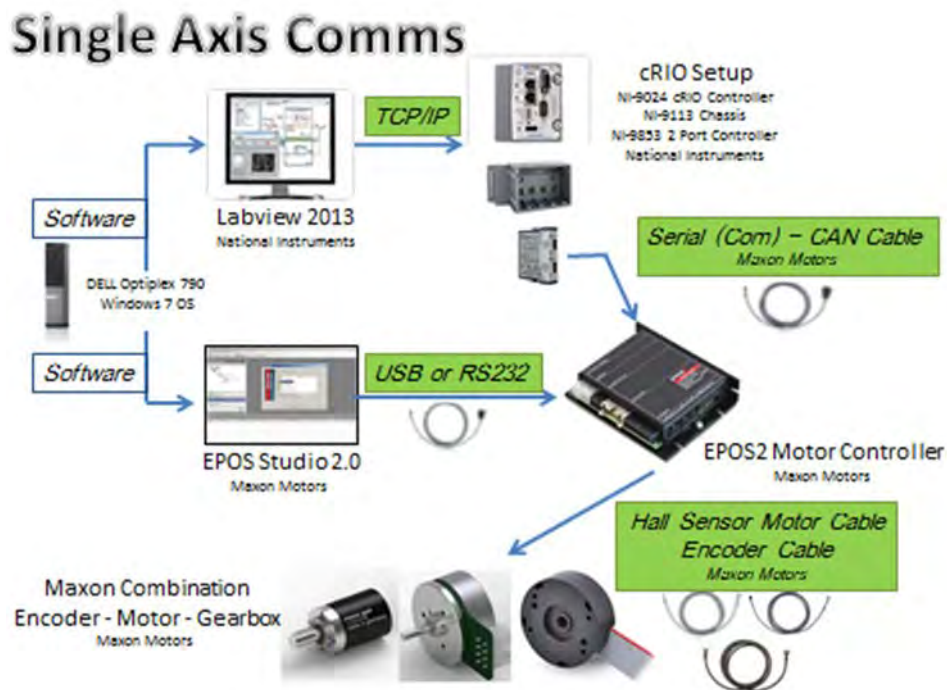
Figure 43.   Single Axis (One Gimbal) Communications Setup

Figure 44 shows the dual axis communications (final setup) of the testbed. The BOM (Table 2) lists the cable part numbers (P/N) and manufacturer. Many of the cables were manufactured in-house. The dual axis communications setup was used to operate multiple

axes simultaneously. For dual axis communications, the LabVIEW program (commanded from the PC) transmits via Ethernet (TCP/IP) to the cRIO, which then transmits via serial-CAN cable to the EPOS2 motor controllers, then transmitting to the motors and gears via (in-house manufactured) hall sensor cables to operate the motor.
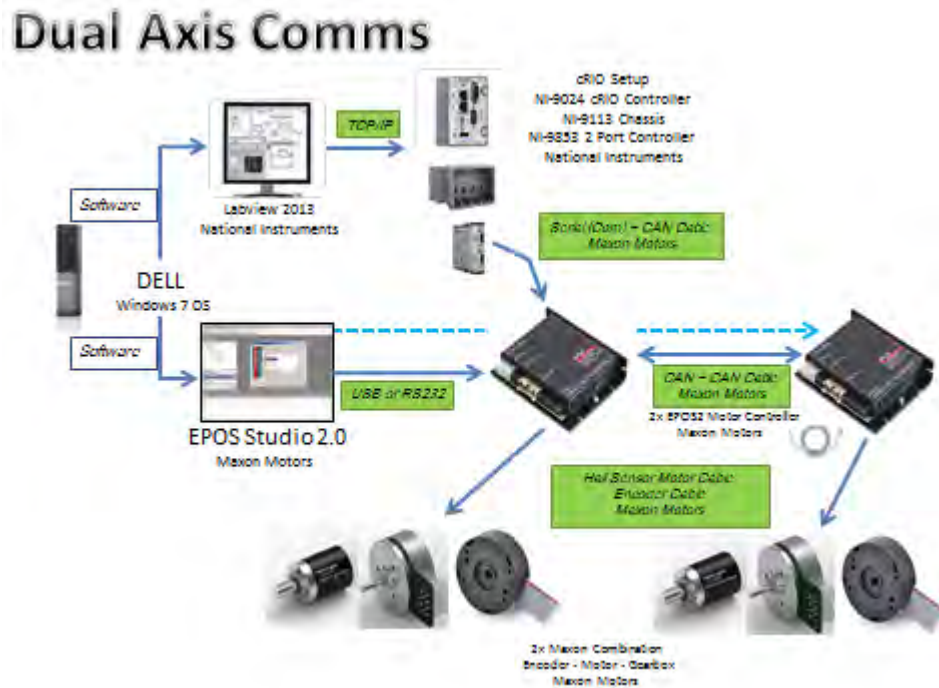
Figure 44.   Dual Axis (Two Gimbal) Communications Setup

2.   Software

a.   *EPOS 2.0 Software*

The EPOS Studio 2.0 is fully functional software downloadable from the Maxon website [16] and a screen shot is shown in Figure 45. EPOS Studio can be used to operate, tune, and run the EC45 motors but has limited functionality. Though limited, the software is very powerful and can be used for many different modes of operation when using the products of EPOS controllers and a variety of different motors from Maxon. The reason for using the LabVIEW software vice the EPOS studio for final implementation is that EPOS studio could not run multiple motors simultaneously while supporting the implementation of arbitrary maneuvers. Any system that did not allow for

multiple axes to be coordinated and/or independently maneuvered was unacceptable as the testbed required AZ and EL to operate independently. Chapter VI describes some alternate methods for dual axis operations using EPOS2 programmable controllers that could be implemented as future work.

Figure 45. EPOS Studio 2.0 Position Mode Screen Shot

b. *CANopen*

CANopen is a communication protocol built upon the controller area network (CAN) physical layer that can be used as an internal bus for embedded devices and motion applications [15]. CANopen communications was used on both EPOS studio and LabVIEW to send commands to the EPOS motor controller via USB or cRIO. Each module includes a 1-port CANopen interface (up to 1Mbit/s) from the NI-9853 and can transmit and receive process data objects (PDO) and service data objects (SDO) according to CiA-DS 301 [15]. According to Cia (CAN in automation), the governing body for CANopen architecture and standards, CANopen is the international standardized application layer for embedded control systems (EN 50323-4). It is one of the most successful communication systems in motion control. CANopen technology comprises several device, interface, and application profiles. Products providing CANopen

connectivity are used in a broad range of applications [17]. In this thesis, CANopen is used to run both gimbals of the prototype antenna simultaneously, and in real-time.

c.   *Windows, NI cRIO (LabVIEW) and Command Software*

The versatility and real-time behavior that was required by the testbed led to lengthy market research into the best software control system for the EPOS controllers. Maxon motors EPOS2 applications guide and technical support representatives recommended several systems that utilized CANopen architecture, but also other methods that include DLL (dynamic link library) drivers and software bit commands. The research showed three promising methods for controlling EPOS2: 1) EPOS Studio 2) LabVIEW software and 3) DLL drivers. Previous research included using MATLAB to send commands to an external device, known as xPC Target as a near real-time system. However, xPC Target was not easily obtainable or supportable. MATLAB also had a VISA-USB system available to send commands, but this approach does not allow for real-time control. Moreover, the research showed it may have never been implemented on EPOS controllers.

All three methods listed above were tested and proved to be promising, and operated on either Windows (Windows 7 OS used) or Linux OS. EPOS Studio provided setup, tuning of motors and maneuvers limited to a single motor at one time or with master-encoder mode two motors running the same input position. EPOS studio did not meet the need of operating two motors in parallel with different position commands. The DLL drivers were tested on a Linux system and were coded based on the EPOS2 DLL drivers available on Maxon Motors website. The Windows DLL is implemented with Microsoft Visual C++ and the library is arranged in groups of functions and helps to simplify the programming of the control software based on Windows [18]. The DLL driver method operated the motors in current mode and is an alternative for future work with multiple EPOS controllers. The Windows DLL supports the SDO protocol from CANopen but the Windows DLL is not qualified for real-time communication [18]. Thus, the method that was chosen was the NI programming method using the LabVIEW software and EPOS drivers for LabVIEW available on both company websites.

45

The EPOS2 drivers for LabVIEW provide VI's (virtual instruments) that communicate and command the EPOS controllers. The VI driver package [19] has EPOS2 examples that operate in different modes such as current, velocity, position and IPM (interpolated position mode) to command the motors via CAN commands to the EPOS2 motor controller. The driver and examples in LabVIEW operate in a LabVIEW project, which executes (deploys) the VI's through communication along the chain of the NI cRIO (NI-9024), chassis (NI-9113), and CAN controller (NI-9853) to the EPOS2. The communication is established with CAN commands through multiple layers of VI's, sub VI's and software controllers. The VI's are embedded and provide for a relatively easy setup and compilation to operate an EPOS2. VI's are two screen operators (front panel and block diagram) as shown in Figure 46 and Figure 47. Figure 46 is the GUI control panel known as a Front Panel, and Figure 47 is the block diagram environment that allows for programming and software communication wiring similar to Matlab Simulink.
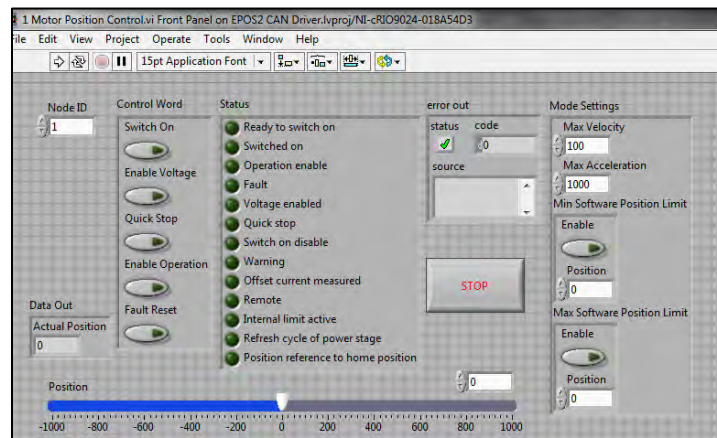
Figure 46.   VI Front Panel for Motor Position Mode (from [20])
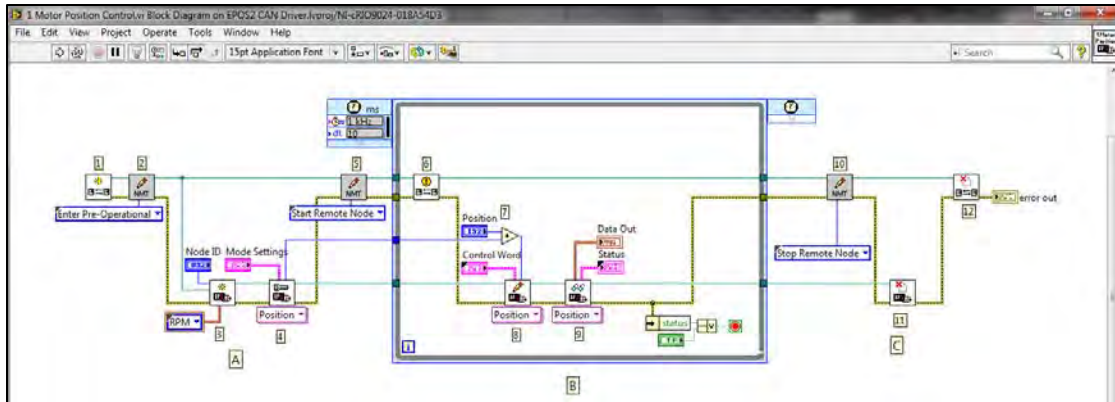
Figure 47.   Block Diagram Panel for Motor Position Mode (from [20])

Throughout the design process, learning and understanding LabVIEW was imperative to generate a system that could operate the motors as intended. After much work, the right software setup was established for compiling the NI-9853 modules and deploying them onto the NI-9024cRIO. This process allowed the NI-9853 to send and receive CAN commands to and from the EPOS2. Once the code could be successfully compiled, the example VI's were manipulated to allow simultaneous operation of the two Maxon EC Flat motors. Initially the tests were run using motors without position encoders, but once the author was satisfied with the control of the motors using the LabVIEW EPOS2 examples, the switch was made to Maxon EC Flat motors with encoders and gear train. Figure 48 and Figure 49 show the final screen shots of the EPOS2 example adaptation with author changes. The changes made to the EPOS2 example VI's were due to the requirement of having two axis controls with individual position trajectories, which led to the final iteration of programming with multiple axis control. The programming inputs or mode settings within the example VI's required minimal inputs to operate the different modes (current, velocity, position, and IPM), each with separate required settings such maximum velocity, acceleration or position limits (each mode of the LabVIEW EPOS2 drivers specific inputs are shown in Section B.1).

47
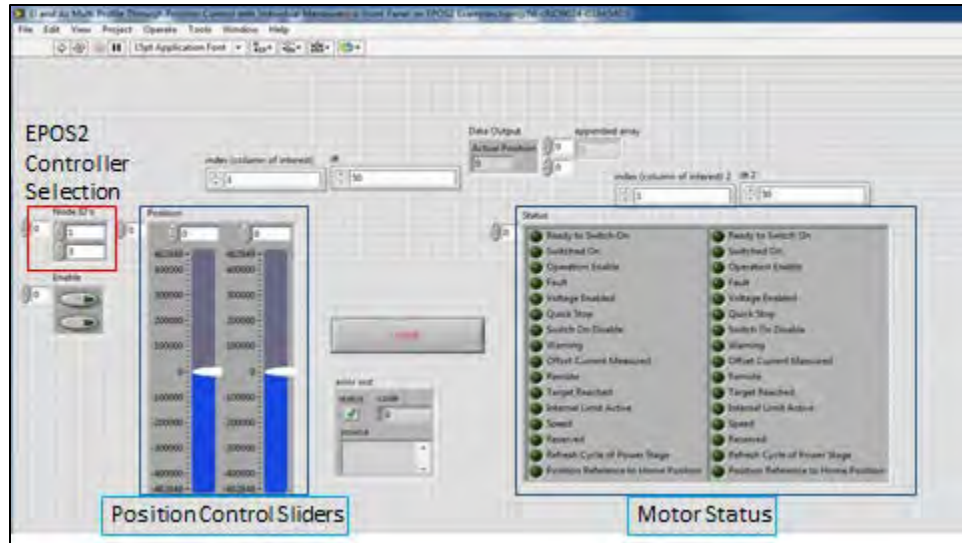
Figure 48.   Screen Shot for the Developed Dual Axis Position Controller Front Panel
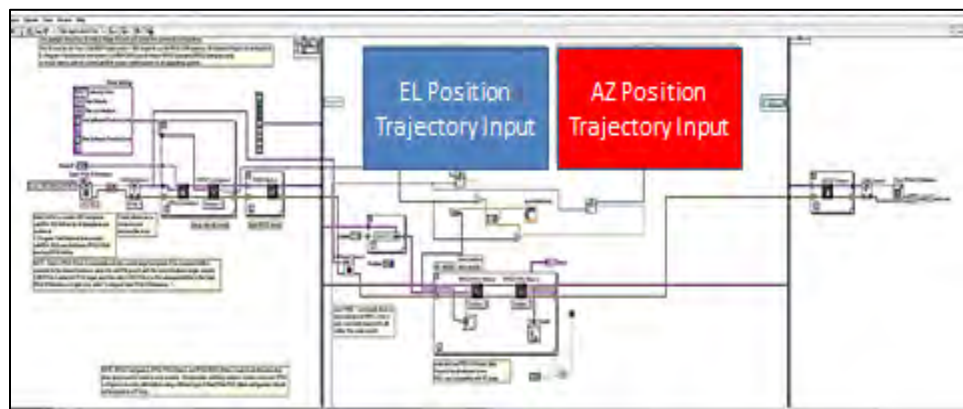
Figure 49.   Screen Shot for the Developed Dual Axis Position Controller Block Diagram

F.   SUMMARY

In this chapter, the testbed hardware and software was integrated to complete the final assembly. The Maxon and NI products greatly contributed to a functional system, though other real-time and motor systems are available that meet requirements set forth in Chapter II. Additionally, a benefit of manufacturing parts for the testbed was using the 3D printer and demonstrating the capabilities of the rapid prototyping process. Finally, in Chapter IV, the software utilizes maneuvering theory to move the motor gimbals.

IV. CONVENTIONAL AND OPTIMAL MANEUVERING: THEORY AND EXPERIMENTS

A. CONVENTIONAL MANEUVERING

Initially the first question to ask is "How does an antenna slew?" To slew an antenna, motors are needed to actuate the motion and to start motor motion; a control system must exist to initiate that motion. This involves motor theory and controls. This chapter describes different methods for providing a closed-loop motor control system with an input to slew the antenna. The system already in place by Maxon Motors is a closed-loop system with the capability to input different signals to alter the output motion of the motors. Some possible methods for altering the motor input for a desired motor output are: 1. Model the desired output as a second order model response. 2. Draw a straight line between the current and desired location and allow the motor control system to select the path (e.g., a step input). 3. Obtain an optimal control path (using the analysis from reference [21]) by solving, for example, the minimum energy maneuvers and provides the solved state trajectory as an input. All three methods can be implemented on the Maxon motors through either EPOS Studio or the LabVIEW software. The reason for altering the motor input trajectories is that the control loops that the EPOS hardware implements are designed for high-gain control. By implementing a second order system model or a trajectory from an optimal controls solution the system can be tuned to run more smoothly. The below sections solve some example maneuver as second order responses or as optimal control solutions to provide trajectories to input into the gimbals.

B. SECOND ORDER MODEL

A controller is a device or sub-system inserted into a system in order to modify the system dynamics. There are many methods used in control systems analysis and design such as; the root-locus method, frequency-response method, the state space method and PID compensation methods [22]. This section describes the implementation of the state space method and PD (position+velocity) compensation to obtain a model second order response that can be used as input to the Maxon control system.

The PD control system is a second-order system that exhibits a range of responses. These responses can be overdamped, underdamped, undamped, or critically damped. Figure 50 shows second order responses for system damping values between zero and two.
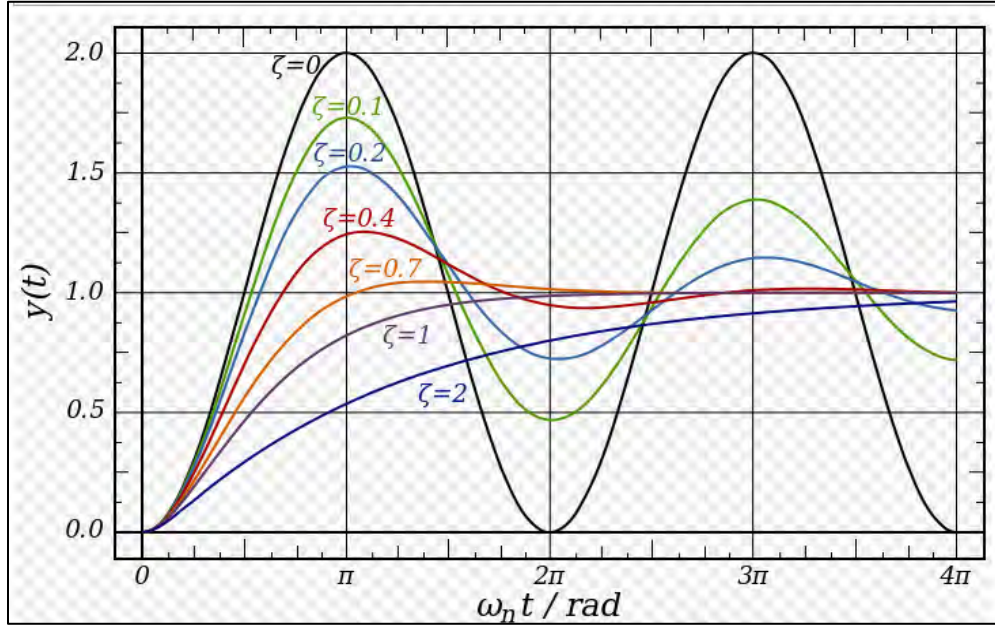
Figure 50. Second Order Responses for Various Damping Ratios

The second order system can be described in states space form as:

$$\dot{x} = Ax + Bu \tag{4.1}$$

$$y = Cx + Du \tag{4.2}$$

The block diagram of the state space system is shown in Figure 51. Where, $\dot{x}$ is a state vector, y is an output signal (scalar), u is the control signal (scalar), A is a [m x m] constant matrix, B is a [m x 1] constant matrix, C is a [1 x m] matrix, and D is a constant (scalar).
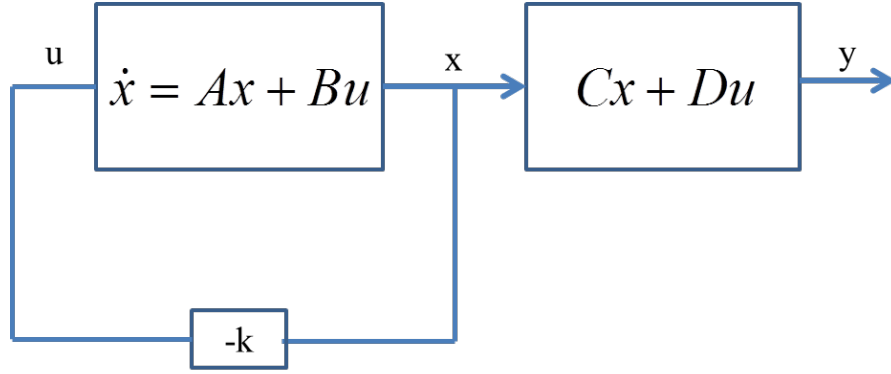
Figure 51.   Second Order Feedback Loop

A maneuvering control system can be modeled using a position + velocity controller or PD controller from a linearized model. By selecting the proportional (P) and derivate (D) gains k_p and k_d where:

$$k_d = \varsigma\omega_n \tag{4.3}$$

$$k_p = \omega_n^2 \tag{4.4}$$

Equations 4.3 and 4.4 can be an input into state space as:

$$u = Kx = \begin{bmatrix} k_p & 0 \\ 0 & k_d \end{bmatrix} x \tag{4.5}$$

The second order system can now be written as:

$$\ddot{e} + u = 0 \tag{4.6}$$

where:

$$u = k_d \dot{e} + k_p e \tag{4.7}$$

This gives:

$$\ddot{e} + k_d \dot{e} + k_p e = 0 \tag{4.8}$$

In Equation 4.8 $e = (x_d - x)$ is the error signal.

51

Equation 4.8 can also be written in the canonical form as:

$$\ddot{e} + 2\zeta\omega_n\dot{e} + \omega_n^2 e = 0$$

(4.9)

To establish the dynamical model for an antenna control system each axis can be modeled as:

$$\sum T = I\alpha = I\ddot{\theta}$$

(4.10)

where I is the moment of inertia about the principal axis of rotation and T is the torque. In this case, the state space model is given by:

$$\dot{\theta} = \omega$$

(4.11)

$$\dot{\omega} = u$$

(4.12)

where:

$$u = T / I$$

(4.13)

The model given in Equations 4.11 and 4.12 is the same as the one described in Equation 4.6 and the same P+V setup can be applied to the antenna control system. Substituting:

$$k_p = k_\theta \text{ and } k_d = k_\omega$$

The control function (u) for a step input is obtained as:

$$u = k_\omega\dot{e} + k_\theta e = k_\omega(0 - \omega) + k_\theta(\theta_d - \theta)$$

(4.14)

The appropriate gains may be determined by using the canonical form of Equations 4.15 and 4.16:

$$k_\omega = 2\zeta\omega_n$$

(4.15)

$$k_\theta = \omega_n^2$$

(4.16)

The damping (ζ) and natural frequency (ω_n) were determined by assuming a criteria of 10 sec settling time (t_s). A settling time of 10 sec was chosen due to the data recording ability of the EPOS system. The t_s was solved using the equations for the two percent criteria interval [21]:

$$t_s = \frac{4}{\zeta \omega_n}$$

(4.17)

System stability is determined by selecting a desired M_p (percent overshoot or OS) of $\leq$ 5 percent (see Equation 4.18). Solving the Equations 4.15, and 4.16 given ζ and ω_n produces the gains k_ω and k_θ. This will be used to design the maneuver to a target time of a 10 sec slew.

$$M_p = e^{\frac{-\zeta \pi}{\sqrt{1-\zeta^2}}}$$

(4.18)

When applying the above equation, the damping was found with Equation 4.19:

$$\zeta = \frac{\left| \ln\left(\frac{M_p}{100}\right) \right|}{\sqrt{\pi^2 + \ln^2\left(\frac{M_p}{100}\right)}}$$

(4.19)

Values of $\zeta \approx .7$ and $\omega_n = .5714$ were solved and plugged into Equations 4.15 and 4.16 to obtain: $k_\omega = .8$ and $k_\theta = .32653$. Figure 52 shows the position (θ) and velocity (ω) versus time for the model second order system with these gains and a slew of 0° to 45°:

53
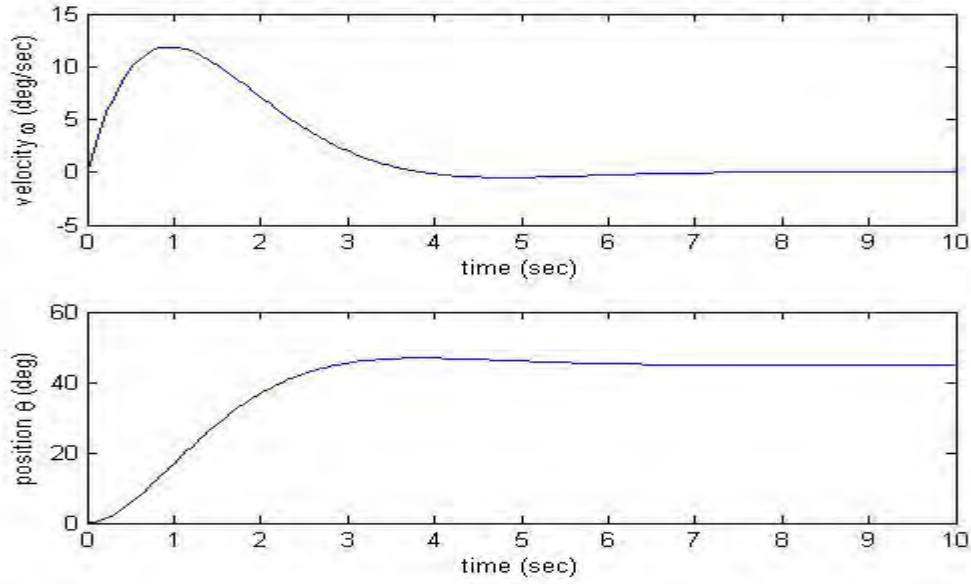
Figure 52.   Example Second Order Response for EL Gimbal (θ and ω)

1.   Implementing the Polynomial Trajectory

The produced control function implies a trajectory has been formed (position and angular velocity that must be reproduced by the motor). As described in Chapter III, the EPOS2 controllers need either a current, position, velocity, or combination of these signals as an input to implement motion on the motors. The requirement for the IPM (interpolated position mode) requires a PVT (position, velocity, time) input. The path or control function produced in the previous section provides the data required for a maneuver. The data implementation, however, can come from any signal. The below sections show the results of the trajectory implementation.

2.   Second Order Response Experiment

The previous section developed the maneuver from rest with $\left(\theta_0,\theta_f\right)=\left(0,45°\right)$ using the second order system model. The purpose of this section is to show that the system can indeed produce the computed trajectory. The position and velocity results were then implemented on the testbed motors for comparison of actual versus commanded values. Thus, the demonstration showed with inputs for position, velocity

54

and current versus time (with position converted to quadcounts (QC)) can be simulated on the testbed. Figure 53 and Figure 54 show the comparison of the actual versus commanded position.

The control function and its exported data (from an excel spreadsheet) must be downstepped into .05sec time steps and into QC for motor operation. The downstepping is taking the time required for the maneuver (in this example 10sec) and breaking down the timesteps into .05sec for the clocking within LabVIEW and provide adequate stepping between position changes. This can be done using the interp1 command in MATLAB for an array of data. The LabVIEW VI does not implement the angular velocity (ω) for each position change as a traditional PVT controller would. To construct the programming for a simulated PVT or IPM mode in LabVIEW, the position mode is used with small incremental timesteps (.05sec) between each position change creating a smooth profile maneuver. Converting the position (θ) from degrees to QC and comparing commanded values to actual values on the testbed are as follows: QC's are calculated by [14]:

$$1024*4*113 = 462849QC \text{ .and } 10\sec/.05\sec = 200steps$$

Where:

$$360° = 462849QC \text{ } (45\deg = 57856QC)$$

After creating the comma separated value (CSV) file from the position, velocity and time, the file is ready for implementation into LabVIEW. The data was recorded using the EPOS studio 2.0. Figure 55 and Figure 56 show the error between the actual position and the commanded position.
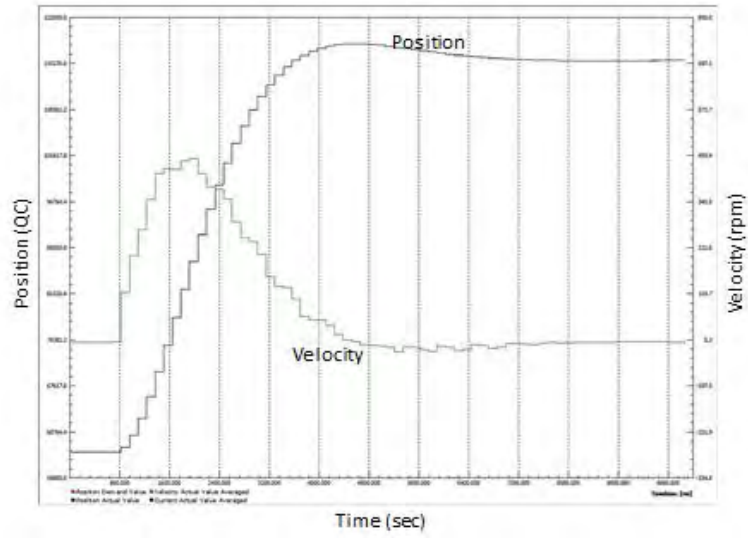
Figure 53.   EL Gimbal Testbed Experiment Response for Second Order Input
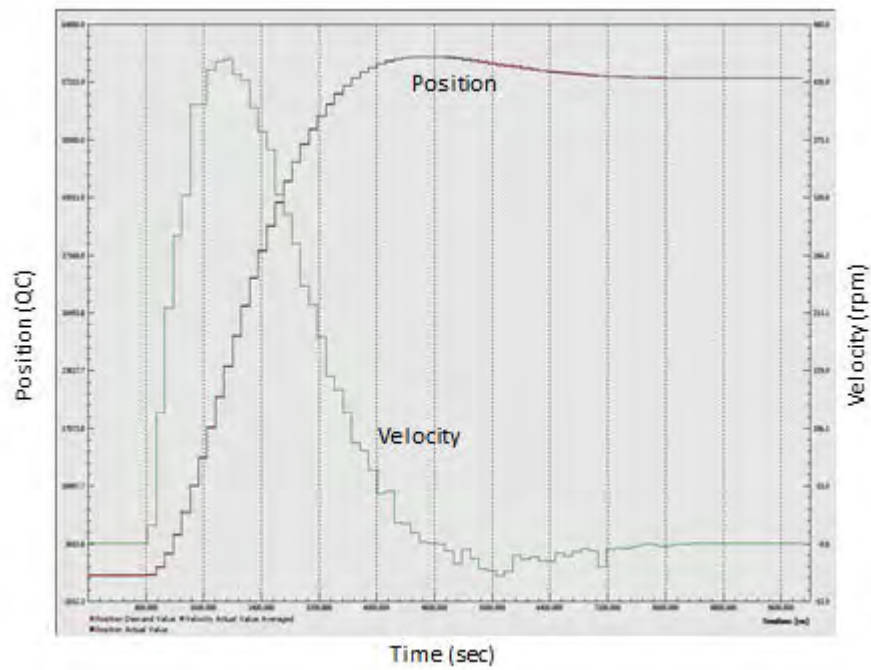
Figure 54.   AZ Gimbal Testbed Experiment Response for Second Order Input

56
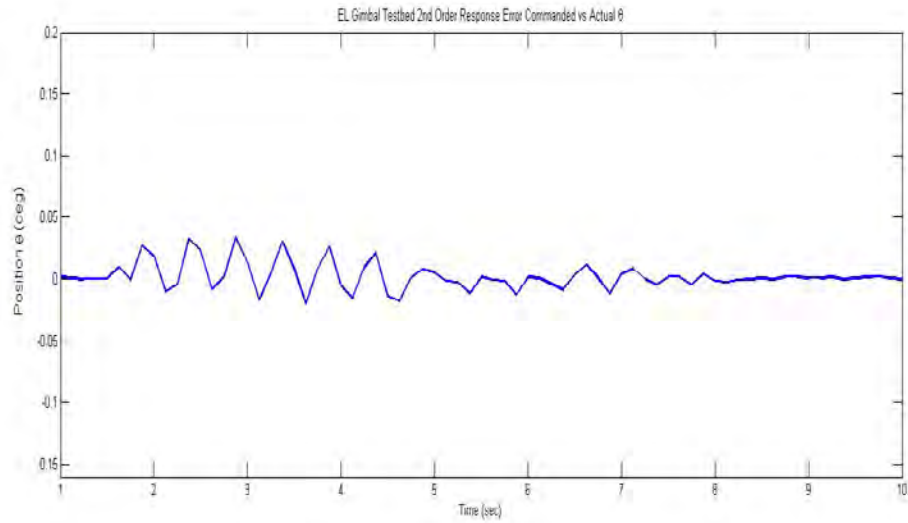
Figure 55.   EL Gimbal Position Error
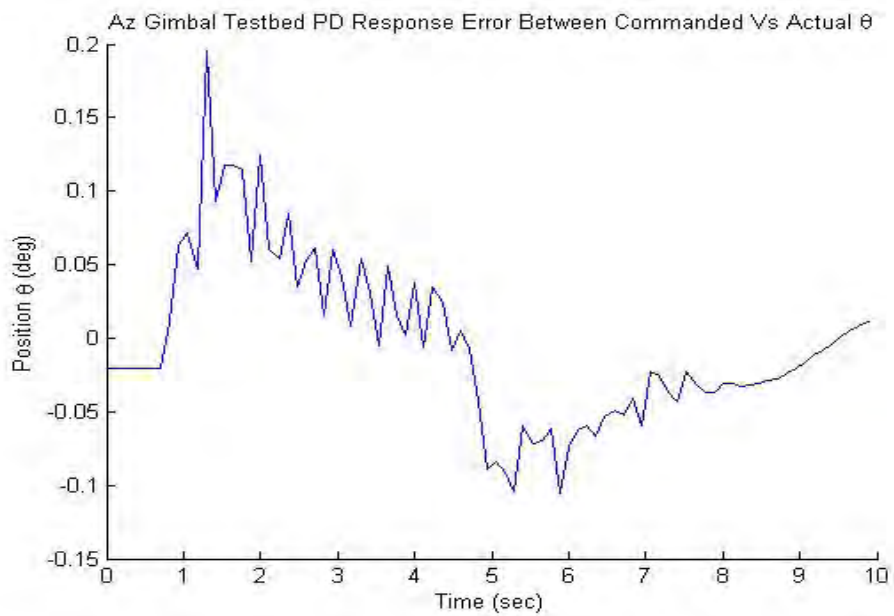
Figure 56.   AZ Gimbal Position Error

The above figures show that the EL gimbal is more accurate than the AZ gimbal, which is expected due to the load on each axis. Figure 57 illustrates the testbed implementing the second order response example in the laboratory.
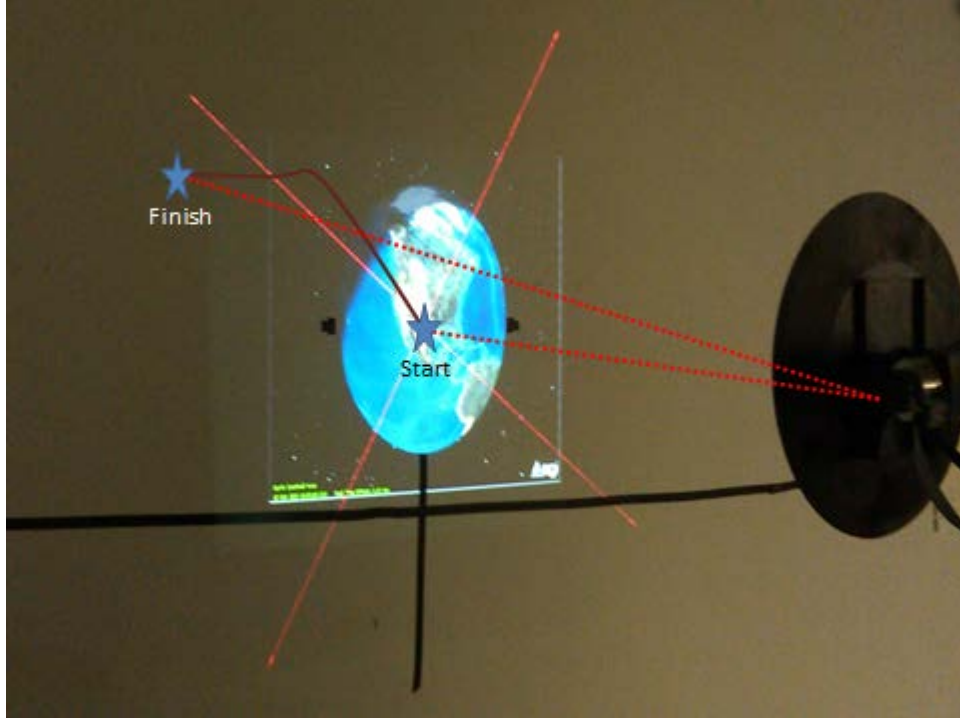
Figure 57.   Example Experiment of Second Order Response Input

C.   MINIMUM ENERGY MANEUVERS

Even though the second order model system can work to produce a path, it may not be the most efficient as compared to the minimum energy maneuver. The minimum energy path has the same bounds as the second order response but uses less energy by modifying the slope of the maneuver trajectory.

As an example, consider a given control function, either a polynomial or in this case a simplified sine wave:

$$u = \sin(t) \ \text{for} \, t \in [0, 2\pi] \tag{4.20}$$

Application for Equation 4.20 gives (for the double integrator plant):

$$\theta(t) = -\sin(t) + t \ \text{where} \, t \in [0, 2\pi] = 2\pi \tag{4.21}$$

$$\omega = -\cos(t) + 1 \ \text{where} \, t \in [0, 1] = 0 \tag{4.22}$$

58

Figure 58 is a plot of the result of the analytical state, control (u) trajectories, and phase space (theta versus omega). Figure 59 illustrates how a trajectory based on the sine wave control input can be simulated in the laboratory. The quadratic cost function (ie energy) for this setup is:

$$J = \frac{1}{2} \int_{t_0}^{t_f} u^2(t) dt$$

(4.23)

When solved, the cost using the sine wave control input was $J = \pi / 2$.
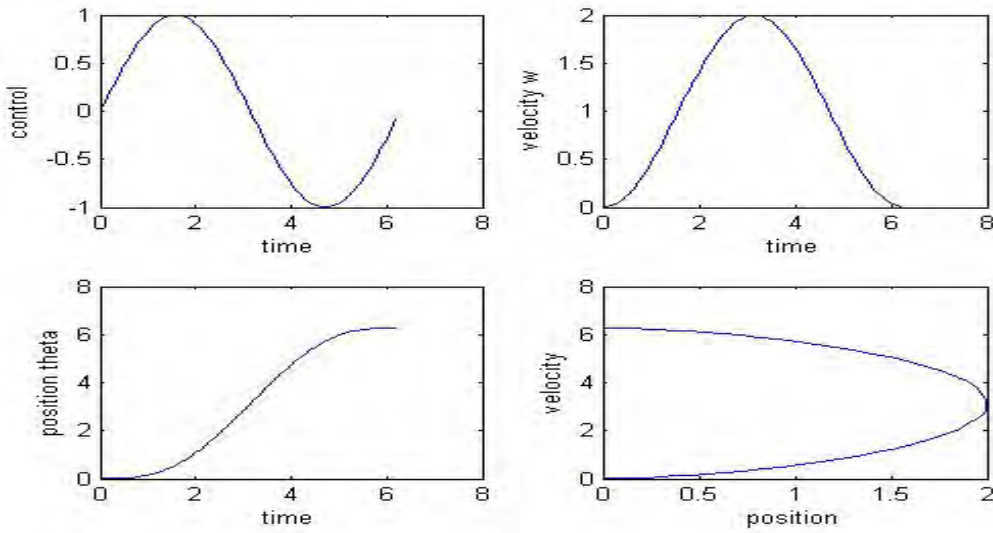
Figure 58.   Minimum Energy Results for Sine Wave Control Function (u)
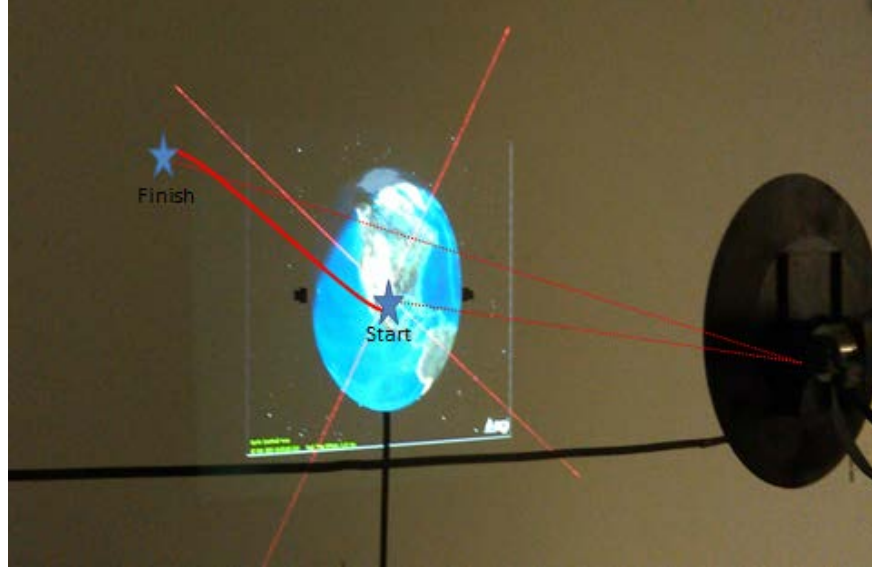
Figure 59.   Testbed Slew Outline on STK for Sine Wave Position Function

The minimum energy maneuvers are governed by the minimizing same cost function as in Equation 4.31, which is the L²-norm of the control [21]. The antenna slew system can be modeled in its simplest form as two double integrators. The model of each axis is:

$$u_{AZ} = \ddot{\theta}_{AZ} = \frac{\tau_{AZ}}{I_{AZ}}$$

(4.24)

$$u_{EL} = \ddot{\theta}_{EL} = \frac{\tau_{EL}}{I_{EL}}$$

(4.25)

The objective is to transfer the system from initial rest position to a final rest position of:

$$(\theta, \omega) = (0, 0) \text{ to } (\theta, \omega) = (45°, 0)$$

Of note: the coupling terms between the two axes (AZ and EL) are ignored and the maneuver does not require the system to start at rest, it could already be in motion and implement a new trajectory (i.e., starting at rest position is arbitrary).

1. Optimal Control of Double Integrators

The solution for the optimal control function introduced in reference [21] takes a stated problem and reduces it to a particular control system trajectory. This trajectory can be used to implement on the testbed's gimbals, either azimuth (AZ) or elevation (EL). The problem statement for minimum energy maneuvering of the testbed model is:

$$x = \left[\theta_{AZ}, \theta_{EL}, \omega_{AZ}, \omega_{EL} \right]^T \in R^4 \tag{4.26}$$

$$u = \left[\alpha_{AZ}, \alpha_{EL} \right] \in R^2 \tag{4.27}$$

Minimize:

$$J\left[\theta(\square), u(\square), t_f \right] = \frac{1}{2} \int_{t_0}^{t_f} u^2(t)\,dt \tag{4.28}$$

Subject to:

$$\dot{\theta}_{AZ} = \omega_{AZ} \tag{4.29}$$

$$\dot{\theta}_{EL} = \omega_{EL} \tag{4.30}$$

$$\dot{\omega}_{AZ} = \alpha_{AZ} = u_{AZ} \tag{4.31}$$

$$\dot{\omega}_{EL} = \alpha_{EL} = u_{EL} \tag{4.32}$$

In the problem formulation above $\dot{\theta}_{AZ}$ is the azimuth rate and $\dot{\theta}_{EL}$ is the elevation rate of the antenna gimbals, and controls u_{AZ} and u_{EL} are the Az and El accelerations (α).

To apply the optimal control solution process described in reference [21] the following steps must be performed:

- Step 1: Construct the Hamiltonian Equation
- Step 2: Construct the Euler-Lagrange Equation
- Step 3: Construct the Adjoint Equation
- Step 4: Establish the Transversality Condition

The above steps frame the testbed problem. In the case below only one gimbal was solved but the solution can be used to represent both gimbals (using AZ below). The equations below are constructed in accordance with the minimum principle process [21]. The boundary conditions are $(\theta_o, \omega_o) = (0,0)$ to $(\theta_f, \omega_f) = (45°, 0)$ and considering the cost function in Equation 4.34 where:

$$x^T = [\theta_{AZ}, \omega_{AZ}], \quad u = [u_{AZ}] = [T_{AZ} / I_{AZ}]$$

(4.33)

Minimize:

$$J[\theta(\square), u(\square), t_f] = \frac{1}{2} \int_{t_0}^{t_f} u^2(t) dt$$

(4.34)

Subject to:

$$\dot{\theta}_{AZ} = \omega_{AZ}$$

(4.35)

$$\dot{\omega}_{AZ} = u_{AZ}$$

(4.36)

$$(\theta_0, \omega_0) = (0,0)$$

(4.37)

$$(\theta_f, \omega_f, t_f) = (45, 0, 10)$$

(4.38)

Establish the Hamiltonian:

$$H = F + \lambda^T f$$

(4.39)

where F is the running cost to give:

$$H\left(\left[\lambda_{\theta_{AZ}}, \lambda_{\omega_{AZ}}\right], [\theta_{AZ}, \omega_{AZ}], [u_{AZ}]\right) := \frac{u_{AZ}^2}{2} + \lambda_\theta \omega_{AZ} + \lambda_\omega u_{AZ}$$

(4.40)

The costates are:

$$\lambda^T := \left[\lambda_{\theta_{AZ}}, \lambda_{\omega_{AZ}}\right]$$

(4.41)

To minimize the Hamiltonian the partial derivative is taken as:

$$\frac{\partial H}{\partial u} = 0 \Rightarrow u + \lambda_{\omega_{AZ}} = 0 \tag{4.42}$$

The adjoint equations are:

$$-\dot{\lambda}_{\theta_{AZ}} = \frac{\partial H}{\partial \theta_{AZ}} = 0 \Rightarrow \lambda_{\theta_{AZ}} = a \tag{4.43}$$

$$-\dot{\lambda}_{\omega_{AZ}} = \frac{\partial H}{\partial \omega_{AZ}} = \lambda_{\theta_{AZ}} \Rightarrow \lambda_{\omega_{AZ}} = -at - b \tag{4.44}$$

Where 'a' and 'b' are constants of integration and in dual space the costate trajectories are straight lines [21].

Since:

$$\lambda_{\omega_{AZ}} = a \tag{4.45}$$

$$u_{AZ} = at + b \tag{4.46}$$

To solve the constants a and b, integrate the control function:

$$\omega = \int \alpha(t) = \frac{1}{2}at^2 + bt + c \tag{4.47}$$

$$\theta = \int \omega(t) = \int \frac{1}{2}at^2 + bt + c = \frac{1}{6}at^3 + \frac{1}{2}at^2 + bt + c + d \tag{4.48}$$

To find the unknown constants a linear system can be solved:

$$\begin{bmatrix} t_0^3/6 & t_0^2/2 & t_0 & 1 \\ t_0^2/2 & t_0 & 1 & 0 \\ t_f^3/6 & t_f^2/2 & 1 & 1 \\ t_f^2/2 & 1 & 1 & 0 \end{bmatrix} \begin{bmatrix} a \\ b \\ c \\ d \end{bmatrix} = \begin{bmatrix} \theta_0 \\ \omega_0 \\ \theta_f \\ \omega_f \end{bmatrix} \tag{4.49}$$

Assuming the boundary conditions are:

$$\theta(t_0, t_f) = (0, 45)° , \omega(t_0, t_f) = (0, 0) \text{ and } (t_0, t_f) = (0, 10)$$

The desired position trajectory becomes (also depicted in Figure 60):

$$\theta(t) = \frac{-.54}{6}t^3 + \frac{2.7}{2}t^2$$

The solution can be used for either AZ or EL gimbal motor inputs if they are both to rotate 45 degrees, or each can be solved independently.
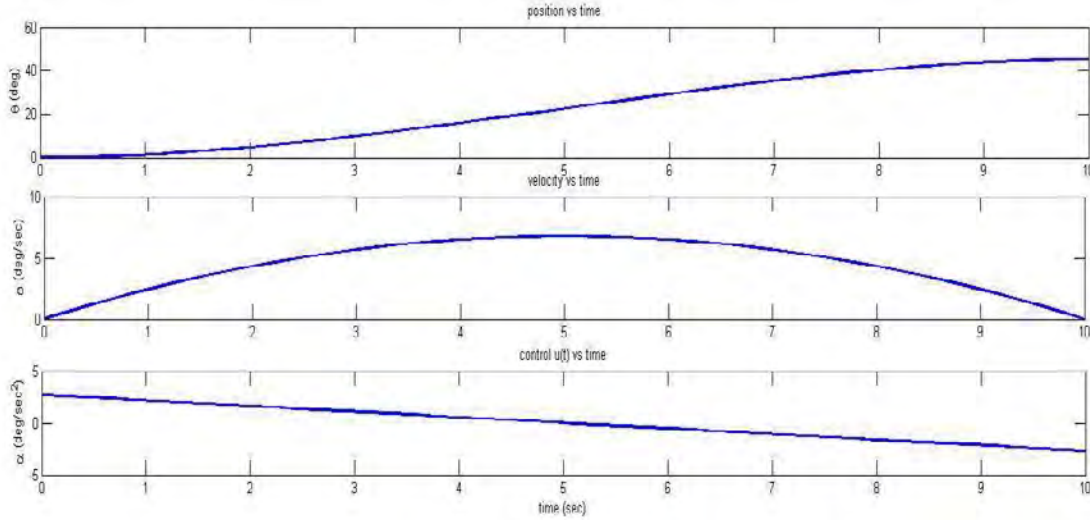
Figure 60.   Desired θ, ω, α Trajectory Obtained from Min Energy Solution

2.   Minimum Energy Maneuver Experiment

The position trajectories from the previous section were implemented on the testbed to show the implementation of an optimal control solution. As before, after creating the CSV file from the position, velocity and time, the file is ready for implementation into LabVIEW. The data is recorded through the EPOS studio 2.0. Figure 61 illustrates the testbed implementing the minimum energy example. Figure 62 to Figure 65 show the commanded versus actual position and the actual velocity and position errors for both gimbals.
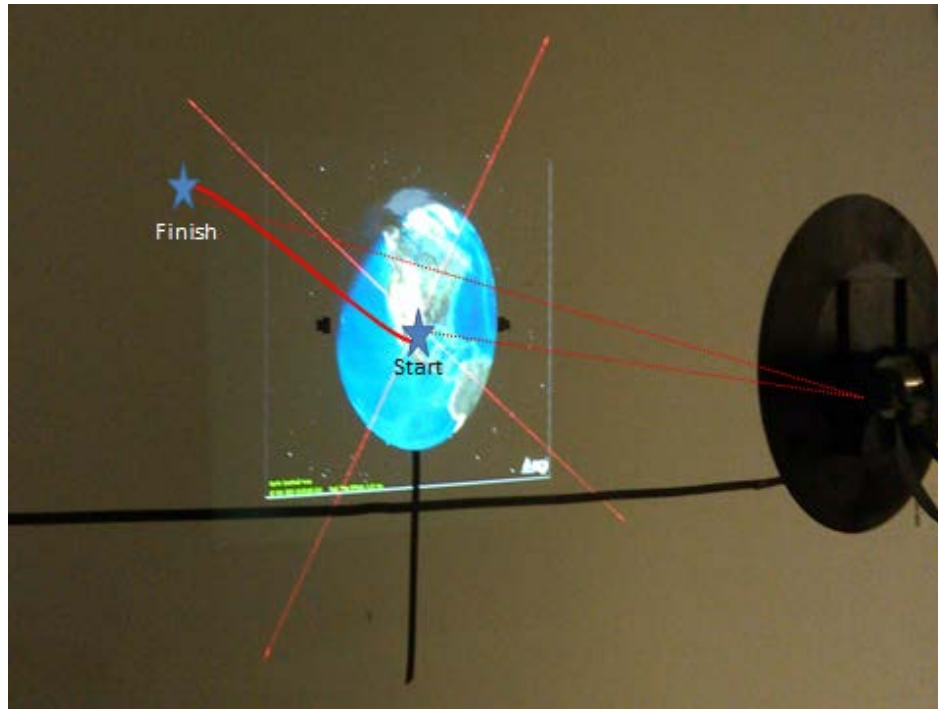
Figure 61.   Example Experiment of Minimum Energy Maneuver
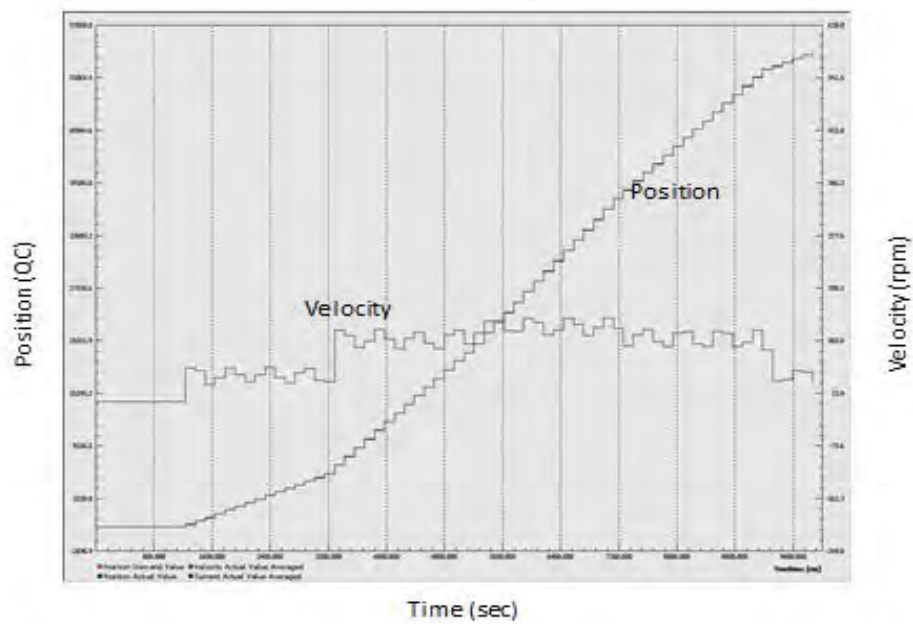
Figure 62.   EL Gimbal Testbed Results for Min Energy Maneuver
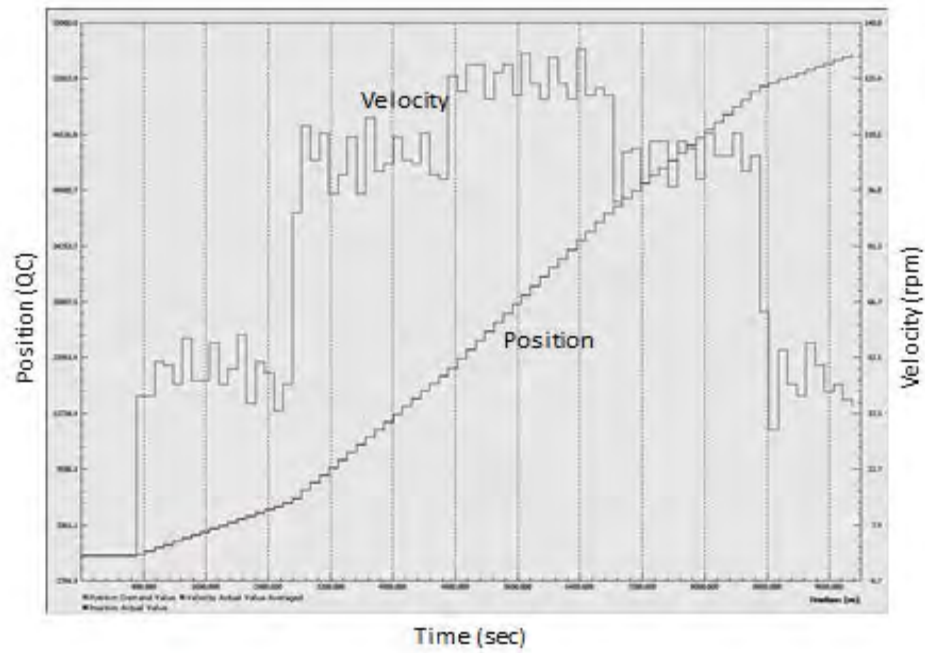
Figure 63.   AZ Gimbal Testbed Results for Min Energy Maneuver
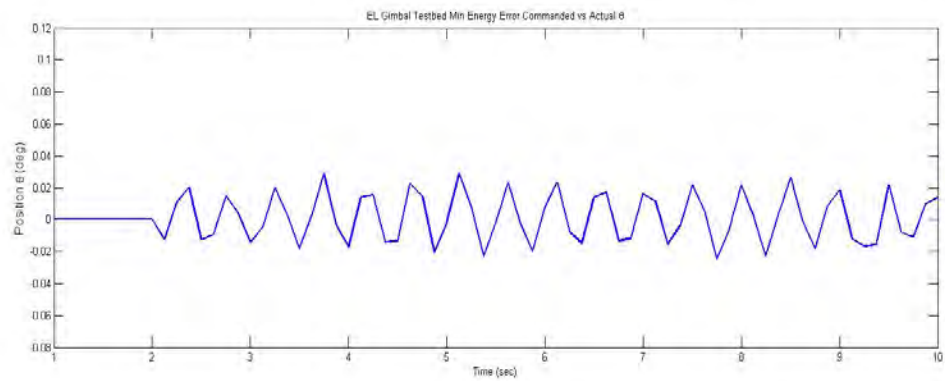
Figure 64.   EL Gimbal Position Error for Min Energy Maneuver
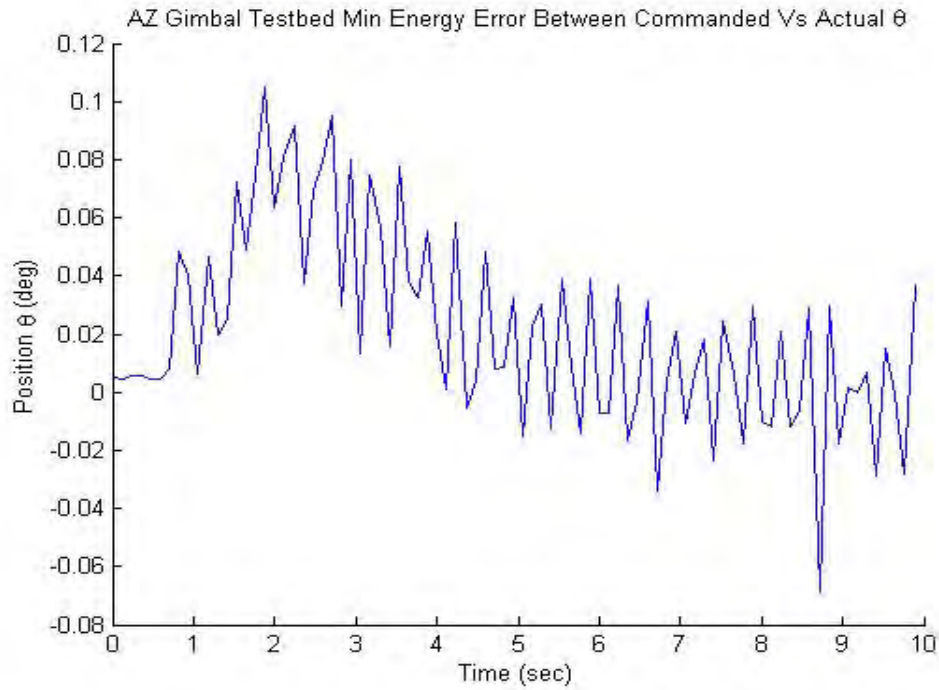
Figure 65.   AZ Gimbal Position Error for Min Energy Maneuver

As demonstrated, arbitrary inputs, whether a sine wave, a linear step, a second order system, or minimum energy control function can be successfully implemented on the testbed. Therefore the testbed can support testing of advance maneuver strategies such as those developed in reference [3].

THIS PAGE INTENTIONALLY LEFT BLANK

V. TESTBED DYNAMIC SCALING EXAMPLES

A. DYNAMIC SCALING

In Chapter II, dynamic scaling, also known as similitude was introduced as a primary focus of the testbed. As described in the introduction, running a simulation on a scaled model vice an on-orbit spacecraft or ground station is cost effective [7], a scaled system is also more simple and inexpensive to operate [6]. On-orbit maneuver testing costs are dramatically high due to operator costs and lost usage time for customers. If a system can be simulated and mimicked on a scaled testbed while not impeding on the current system's contracted time it will save money and time for the full scale operation. In order to create a dynamically equivalent testbed similar to a full size antenna arm or ground station, all essential parameters of the scaled testbed must be matched as closely as possible with those of full sized system by using dimensional analysis and scaled matrix operations. The testbed utilizes dynamic scaling by scaling dynamic equations (scaled inertia tensor and torque). The testbed has its own characteristics in the form of mass and inertia properties. The full sized antenna arm will also have its own inertia properties. To scale a full size antenna to the testbed, the inertia tensor or torques must be scaled in a way that provides the best possible emulation of the real (full scale) system. The motion of the gimbals is described by:

$$\sum T = I\alpha$$

(5.1)

The torque of the gimbal requires the inertia of the system. The testbed inertia properties are estimated using the Solidworks inertia calculator due to the complexity of the build and shape of the testbed assembly. Equations 5.2 to 5.8 show the Solidworks method for solving the values of the inertia tensor matrix [23].

$$I = \begin{bmatrix} I_{xx} & -I_{xy} & -I_{xz} \\ -I_{xy} & I_{yy} & -I_{yz} \\ -I_{xz} & -I_{yz} & I_{zz} \end{bmatrix}$$

(5.2)

where:

$$I_{xx} = \int \left(y^2 + z^2 \right) dm$$

<div align="right">(5.3)</div>

$$I_{yy} = \int \left(z^2 + x^2 \right) dm$$

<div align="right">(5.4)</div>

$$I_{zz} = \int \left(x^2 + y^2 \right) dm$$

<div align="right">(5.5)</div>

$$I_{xy} = \int \left(xy \right) dm$$

<div align="right">(5.6)</div>

$$I_{zx} = \int \left(zx \right) dm$$

<div align="right">(5.7)</div>

$$I_{yz} = \int \left(yz \right) dm$$

<div align="right">(5.8)</div>

1.   Complete Testbed Scale Model and Inertia Properties

The center of mass of the entire testbed is illustrated in Figure 66 and in Table 5. The testbed's inertia values (I) can be represented by three methods: 1) Principal axes of inertia and principal moments of inertia given in Table 6 and taken at the center of mass (kg•mm²). 2) Moments of inertia (taken at the center of mass and aligned with the output coordinates system) (kg•mm²) and 3) Moments of inertia (taken at the output coordinate system) (kg•mm²) as shown for the entire testbed and each body (see Equations 5.9, 5.10, 5.13, 5.14, 5.15, and 5.16). The volume of the testbed assembly is 8,741,603 (mm³) or 0.008741603 m³. The mass is 8.9566 kg by CAD design, the actual mass is 9.422 kg. The difference of mass (<5 percent) is due to the fasteners and cable weight not being accounted for in the CAD (Solidworks) model.
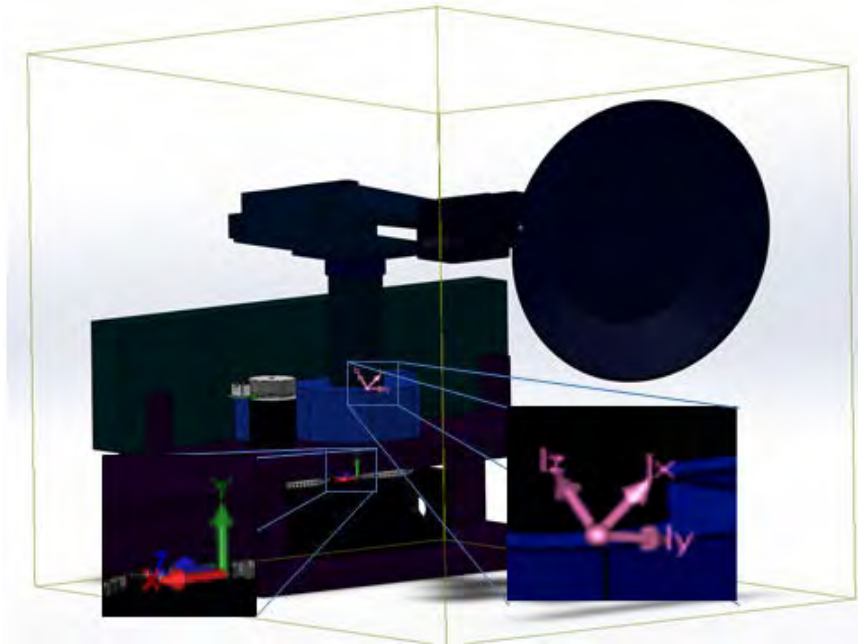
Figure 66.   Complete Assembly with Principal Axis Shown

	Center of Mass (mm)
X	-5.6553
Y	96.33
Z	-9.5465

Table 5.   Testbed Center of Mass

Principal Unit Vector			
Ix	-0.1622	0.7369	-0.6561
Iy	-0.9833	-0.1762	0.0452
Iz	-0.0823	0.6525	0.7532
Principal Moments of Inertia (kg·mm²)			
Px	80767.5		
Py	175402.8		
Pz	191142.2		

Table 6.   Principal Axis of Inertia and Principal Moments of Inertia

For the entire testbed, Equation 5.9 gives the moments of inertia (in kg•mm²) taken at the center of mass and aligned with the output coordinate system (shown in Figure 66) and Equation 5.10 are the moments of inertia (in kg•mm²) taken at the output

coordinate system. A description of these outputs with respect to the reference frame (output coordinate frame) of the testbed is described in reference [23].

$$L = \begin{bmatrix} L_{xx} & L_{xy} & L_{xz} \\ L_{xy} & L_{yy} & L_{yz} \\ L_{xz} & L_{yz} & L_{zz} \end{bmatrix} = \begin{bmatrix} 173017.2 & -10472.7 & 11052.5 \\ -10472.7 & 130703.7 & -53498.8 \\ 11052.5 & -53498.8 & 143591.6 \end{bmatrix}$$

(5.9)

$$I = \begin{bmatrix} I_{xx} & I_{xy} & I_{xz} \\ I_{xy} & I_{yy} & I_{yz} \\ I_{xz} & I_{yz} & I_{zz} \end{bmatrix} = \begin{bmatrix} 256946.3 & -15352.1 & 11536.1 \\ -15352.1 & 131806.5 & -61735.4 \\ 11536.1 & -61735.4 & 226990.9 \end{bmatrix}$$

(5.10)

2.   Multi-body Inertia Properties

To create a modular, scalable, and universal testbed that can mimic most two-axis gimbal antenna systems, "all of the elements of inertia's and torques must be carefully measured and positioned" [6]. A system of dynamic equations requires input inertias, masses, and distances from Center of Mass (CoM) to each connecting joint [24]. A typical joint between multiple links are illustrated in Figure 67. Table 7 lists the units for inertia and torque.
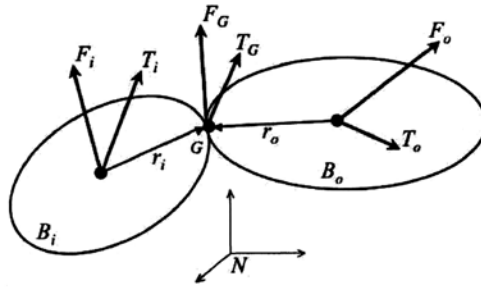

Figure 67.   Two Bodies Connected By A Spherical Joint (from [24])

The rotational motion of a rigid body is governed by Euler's equation:

$$I\dot{\omega} = T - \omega \times H$$

(5.11)

where:

$$H = I\omega \qquad (5.12)$$

From Equation 5.11 and substituting in Equation 5.12:

$$I\dot{\omega} = T - \omega \times I\omega \qquad (5.13)$$

	Units
Moments of Inertia	kg·mm²
Torque	kg·mm/sec²

Table 7.　　Units of Inertia and Torque

In Equation 5.13, $\dot{\omega}$ is the angular acceleration, ω is the angular velocity, and H is the angular momentum. Stoneking's approach [24] to constructing the dynamic equations generalizes a system into N bodies, with each body having its own center of mass and inertia properties. Each body, or member, or joint has a distance between the principal axis from the CoM and can be separated at the joint connection (rotational center of the gimbal). In this framework, the testbed can be modeled as three bodies with each body's rotational motion described in Equation 5.11, refer to reference [25] for further details. Bodies three and two are shown in Figure 68 and Figure 69, respectively. Body three begins from the moving components of the elevation gimbal. Body two includes all the azimuth moving components that do not include body three or body one. Body one is any component not moving due to the elevation or azimuth gimbal (i.e., the base, EPOS2 controllers, NI system, etc.)
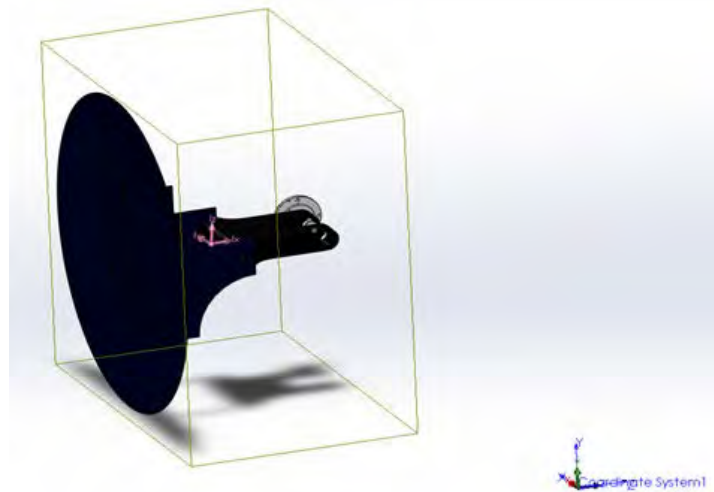
Figure 68.   Body 3—Components Illustrated

Body three, moments of inertia is estimated from Solidworks as:

	Center of Mass (mm)		
X	-5.554		
Y	292.1		
Z	-315.8		
Principal Unit Vector			
Ix	0.1954	-0.0577	0.979
Iy	0.98	0.0481	-0.1928
Iz	-0.036	0.9971	0.066
Principal Moments of Inertia (kg·mm²)			
Px	675.1		
Py	839.7		
Pz	885.9		

Table 8.   Body 3—Center of Mass and Inertia Values

For body three, Equation 5.14 are the moments of inertia taken at the center of mass and aligned with the output coordinate system. Equation 5.15 are the moments of inertia taken at the output coordinate system.

$$L = \begin{bmatrix} L_{xx} & L_{xy} & L_{xz} \\ L_{xy} & L_{yy} & L_{yz} \\ L_{xz} & L_{yz} & L_{zz} \end{bmatrix} = \begin{bmatrix} 833.5 & -.1977 & 31.61 \\ -.1977 & 885.1 & -12.33 \\ 31.61 & -12.33 & 682.2 \end{bmatrix} \qquad (5.14)$$

$$I = \begin{bmatrix} I_{xx} & I_{xy} & I_{xz} \\ I_{xy} & I_{yy} & I_{yz} \\ I_{xz} & I_{yz} & I_{zz} \end{bmatrix} = \begin{bmatrix} 29133.9 & -248.3 & 299.8 \\ -248.3 & 16143.1 & -14119.5 \\ 299.8 & -14119.5 & 13734.1 \end{bmatrix} \qquad (5.15)$$
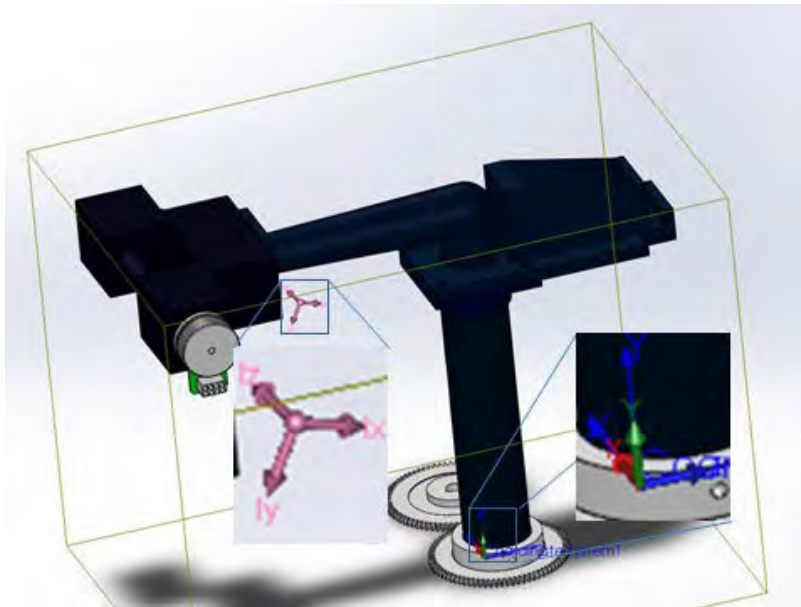

Figure 69.   Body 2—Component Illustration

Body two, moments of inertia is estimated as:

	Center of Mass (mm)		
X	-32.87		
Y	259.7		
Z	-127.1		
Principal Unit Vector			
Ix	0.2302	-0.4038	0.8853
Iy	0.0321	-0.9062	-0.4217
Iz	0.9726	0.1255	-0.1957
Principal Moments of Inertia (kg·mm²)			
Px	9379.4		
Py	30251.9		
Pz	33177.4		

Table 9.   Body 2—Center of Mass and Inertia Values

For body two, Equation 5.16 are the moments of inertia taken at the center of mass and aligned with the output coordinate system and Equation 5.17 are the moments of inertia taken at the output coordinate system.

$$L = \begin{bmatrix} L_{xx} & L_{xy} & L_{xz} \\ L_{xy} & L_{yy} & L_{yz} \\ L_{xz} & L_{yz} & L_{zz} \end{bmatrix} = \begin{bmatrix} 31912.8 & -2298.0 & 4811.7 \\ -2298.0 & 26893.8 & -7391.3 \\ 4811.7 & -7391.3 & 14002.2 \end{bmatrix}$$

(5.16)

$$I = \begin{bmatrix} I_{xx} & I_{xy} & I_{xz} \\ I_{xy} & I_{yy} & I_{yz} \\ I_{xz} & I_{yz} & I_{zz} \end{bmatrix} = \begin{bmatrix} 169068.6 & -16304.9 & 11664.7 \\ -16304.9 & 55157.0 & -61535.3 \\ 11664.7 & -61535.3 & 126440.5 \end{bmatrix}$$

(5.17)

Table 10 shows the volume and mass of each body (used in later calculations).

	Body 3	Body 2
Mass (Kg)	0.1529	1.641
Volume (mm³)	202384.6	1244165.4

Table 10.   Body Three and Two Mass and Volume

3.   Scaling Methods

A scale factor must be introduced to scale inertia values of a full size antenna system to the testbed. Through research, this thesis presents two ways to scale the data

obtained from the testbed to represent the dynamics from a full scale antenna (2-axis gimbals AZ and EL) and to satisfy Equation 5.13. The methods for scaling data for each body are:

a.   Method 1

Change the inertia values of the testbed by adding mass at points to account for the inertia scale factor (SF), which matches the radii of gyration (see before and after in Figure 70 and Figure 71, respectively) thereby scaling the full scale antenna to the testbed and satisfying Equation 5.18. Data collected from the full scale and prototype bodies can be simply corrected by scaling the original testbed. The initial radii of gyration are calculated using Equation 5.19. The SF can be used to solve for a new set of points for radii of gyration (see Equation 5.20). This is not the preferred method because it is extremely difficult to keep the testbed operating and mass has to be constantly added to collect data, thus constantly changing the prototype's inertia characteristics [7].
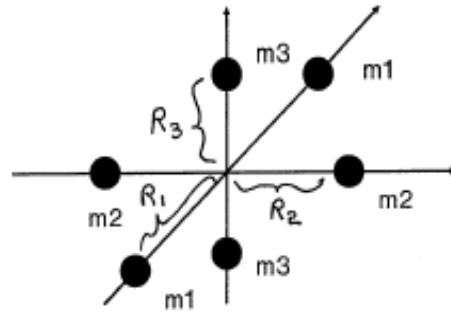

Figure 70.   Prototype Before Scaling Radius of Gyration Point Mass Assumption (from [7])
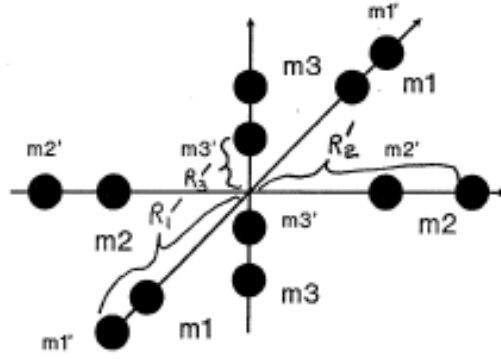
Figure 71. Prototype After Scaling Radius of Gyration Point Mass Assumption (from [7])

$$\begin{bmatrix} I_{xx} & -I_{xy} & -I_{xz} \\ -I_{xy} & I_{yy} & -I_{yz} \\ -I_{xz} & -I_{yz} & I_{zz} \end{bmatrix}_{FullScale} = SF_I * \begin{bmatrix} I_{xx} & -I_{xy} & -I_{xz} \\ -I_{xy} & I_{yy} & -I_{yz} \\ -I_{xz} & -I_{yz} & I_{zz} \end{bmatrix}_{Testbed}$$

(5.18)

$$r_{TB_{original}} = \sqrt{\frac{I_{TB_{Body}}}{m_{Body}}}$$

(5.19)

$$r_{TB\,new} = SF_I * r_{TB_{original}}$$

(5.20)

Where $r_{TB_{original}}$ is the original radii of gyration for the testbed body components and $r_{TB\,new}$ is the new radii of gyration (mm) and SF_I is the SF for the body component and is a 3x3 matrix.

b.   Method 2

Stoneking introduces the Newtonian dynamic equation (Equation 5.13) for an individual body component as [24]:

$$I_i \dot{\omega}_i = T_i - \omega_i \times H_i + T_G + r_i \times F_G$$

(5.21)

Where a control torque $T = u(t)$ can be interpreted as the summation of T_i (an external torque and is negligible), the T_G (the torque of the gimbal), and the $r_i \times F_G$ term (the torque arising from the constraint force at the joint). From Equation 5.21 both the full scale and testbed body components are established in differential form to solve for:

angular velocity ω(t), the control function u(t), and angular acceleration $\dot{\omega}$, the full scale and testbed body components differential as a function of time are shown in Equation 5.22 and 5.23:

$$\left[I\frac{d\omega}{dt} - u + \omega \times I\omega \right]_{Fullscale} = 0 \tag{5.22}$$

$$\left[I\frac{d\omega}{dt} - u + \omega \times I\omega \right]_{Testbed} = 0 \tag{5.23}$$

To attempt to make Equations 5.22 and 5.23 equivalent, it is possible to equate acceleration terms as:

$$I_{FS}\dot{\omega}_{FS} = I_{TB}\dot{\omega}_{TB} \tag{5.24}$$

Therefore:

$$\dot{\omega}_{TB} = \left[I_{TB}\right]^{-1} I_{FS}\dot{\omega}_{FS} \tag{5.25}$$

$$\omega_{TB} + \omega_{TB_0} = \int \dot{\omega}_{TB} \tag{5.26}$$

$$u_{TB} = I_{TB}\dot{\omega}_{TB} + \omega_{TB} \times I_{TB}\omega_{TB} \tag{5.27}$$

By solving for the full scale bodies angular velocity ω(t), the control function u(t), and angular acceleration $\dot{\omega}(t)$ as a function of time the results becomes an input (Equation 5.24) to the control application of the testbed and in extension the EPOS2 drivers (refer to Chapter IV), consequently the testbed mimics the full scale system. The next section implements an example of the above methods and steps for the dynamic scaling of a full scale antenna system to the testbed antenna system.

B.   ANTENNA SYSTEM SIMILITUDE EXPERIMENTS

The following section presents some illustrative application of both methods introduced for scaling a full scale (real) system described in the last section. Initially to scale a real system, a real system has to be chosen that has an antenna and ideally two gimbals (AZ and EL) or a system that creates gimbal joint bodies to mimic. To gather the data (from an operating or in development system) the author had to seek out systems

discussed in Chapter II. For example, the Tracking and Data Relay Satellite (TDRS), a NASA communications satellite, was researched and was the focus of the below experiments. As discussed in Chapter IV to use the testbed, a slew trajectory has to be determined for implementation on the gimbal motors. In addition, to implement either method, component data is needed to satisfy the initial data for solving Equation 5.18 in method one and Equation 5.21 in method two. The below sections applies TDRS data (from reference [26]) to implement an example of the proposed methods.

1.   Proposed Data and Implementation of Dynamic Scaling

TDRS is a two axis system driven by identical motor drive assemblies and that are joined by a gimbal structure resulting in an elevation over azimuth configuration [26]. Other systems, similar to TDRS, such as LANDSAT-D [27], which has two-axis gimbals (Ku antennas) could also be mimicked. The TDRS S-Band single axis antennas have the approximate parameters for the bodies three and two (shown in Table 11 and Table 12); the system is shown in Figure 72:

	TDRS Body 3 Inertia's (kg·m²)		
Ix	10	0.5	0
Iy	0.5	15	0.1
Iz	0	0.1	11

Table 11.   TDRS Body Three Inertia Values (from [26])

	TDRS Body 2 Inertia's (kg·m²)		
Ix	2	0.1	0
Iy	0.1	3	0.02
Iz	0	0.02	2.2

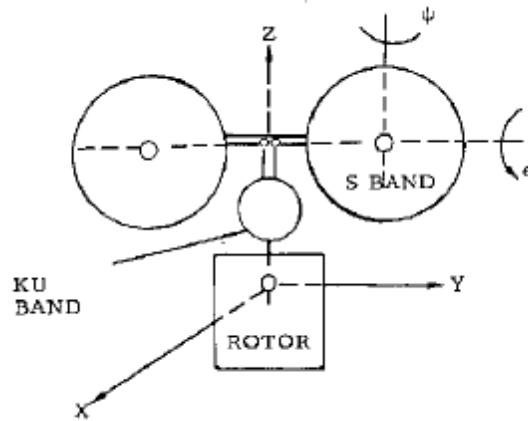Table 12.   TDRS Body Two Inertia Values (from [26])

Figure 72.   TDRS Antenna Setup (from [26])

a.   Method 1

As described in Section A.3., method one implements Equations 5.18 to 5.20 to solve new radii of gyration points of the scaled system. However as mentioned previously, this is not the preferred method because it is extremely difficult to keep the testbed operating and mass has to be constantly added to collect data. This impairs meeting the requirement of a modular testbed (see Chapter II). Implementing Equations 5.18 to 5.20 gives the scale radii of gyration shown in Table 13 and Table 14, and plotted in Figure 73 to Figure 76.

Body 3 Scaled Radii of Gyration (mm)		
rx	1.3	0.1	0.1
ry	0.0	0.6	0.6
rz	0.1	0.8	0.8

Table 13.   Body 3 Scaled Solution for Radii of Gyration

Body 2 Scaled Radii of Gyration (mm)		
rx	28.22	10.68	9.86
ry	4.30	7.42	9.24
rz	9.30	16.72	21.73

Table 14.   Body 2 Scaled Solution for Radii of Gyration
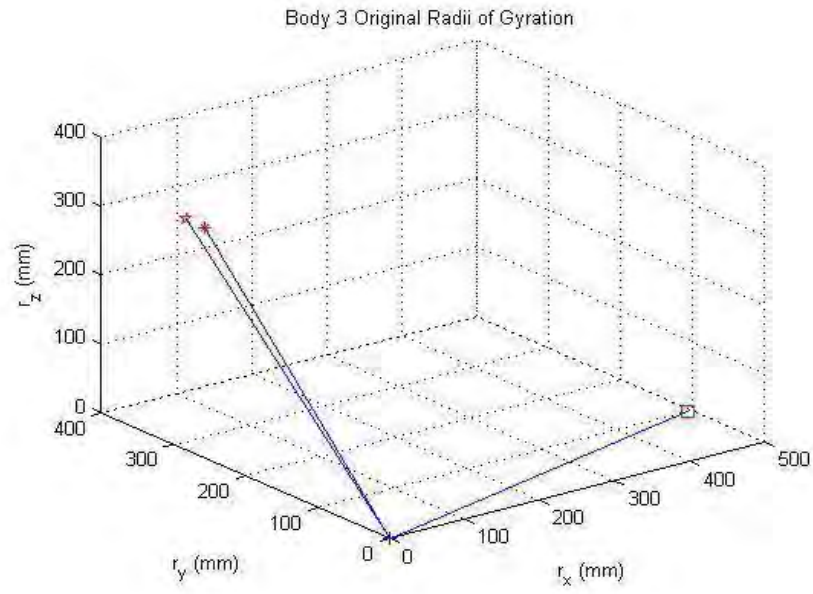
81

Figure 73.   Body 3 Original Radii of Gyration (TDRS Example)
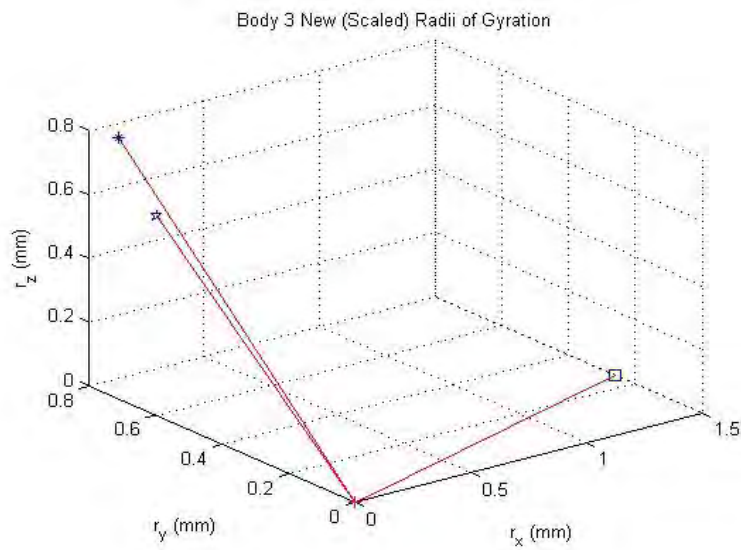

Figure 74.   Body 3 New (Scaled) Radii of Gyration (TDRS Example)
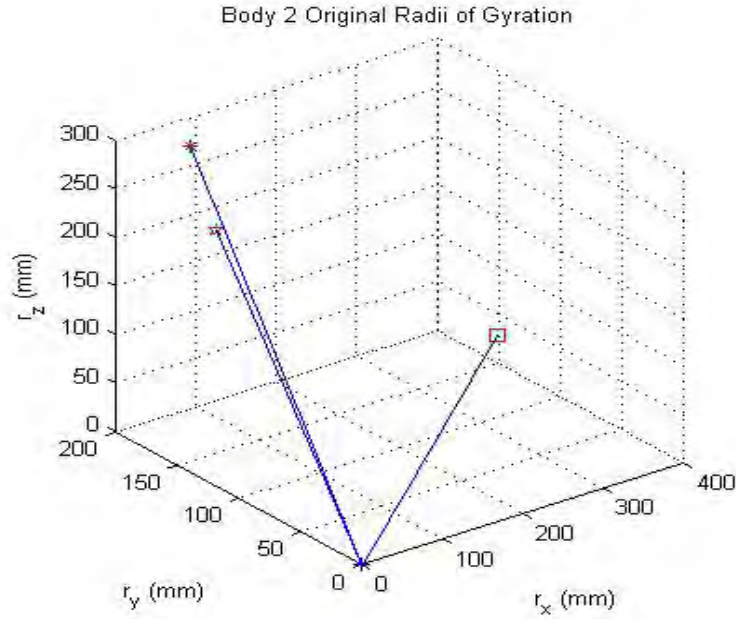
Figure 75.   Body 2 Original Radii of Gyration (TDRS Example)
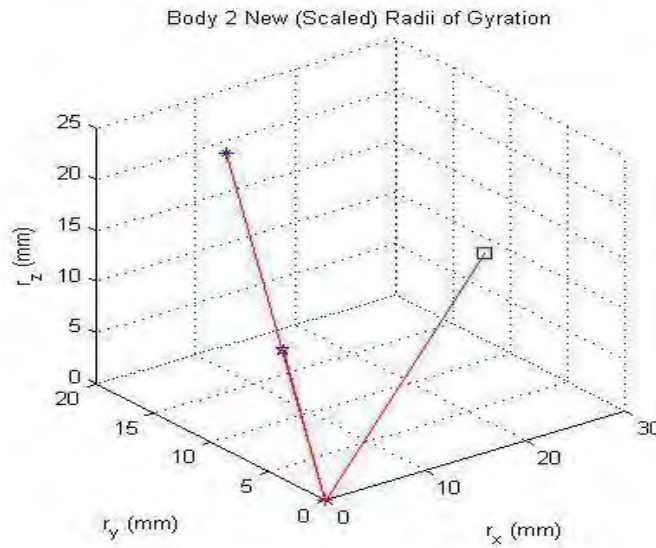

Figure 76.   Body 2 New (Scaled) Radii of Gyration (TDRS Example)

Based on the results for method one, it can be seen that it is not preferred because the new radii of gyration are extremely small. This makes it extremely difficult to match the testbed inertias (making it difficult to scale data). Reference [7] came to the same conclusion for this method in a different application.

As described in Section A.3, method two implements Equations 5.21 to 5.28 and solves the differential equation of the Newtonian dynamics of the full scale system and inputs the dynamic system states solution as an input to the testbed angular dynamic system states therefore solving the scaled angular acceleration (and by extension angular velocity) needed for the output of the testbed torques. These output torques can be implemented on the testbed motors (as in Chapter IV), and are determined in the following section. Again, using TDRS data from reference [26] for inertia values and implementing the solution for an optimal control solution of Equation 5.22 from reference [25] into Equation 5.24 (reordered in Equation 5.25) and Equation 5.26 provides the results for method two. Figure 77 to Figure 80 illustrate the implementation of method two on bodies three and two.
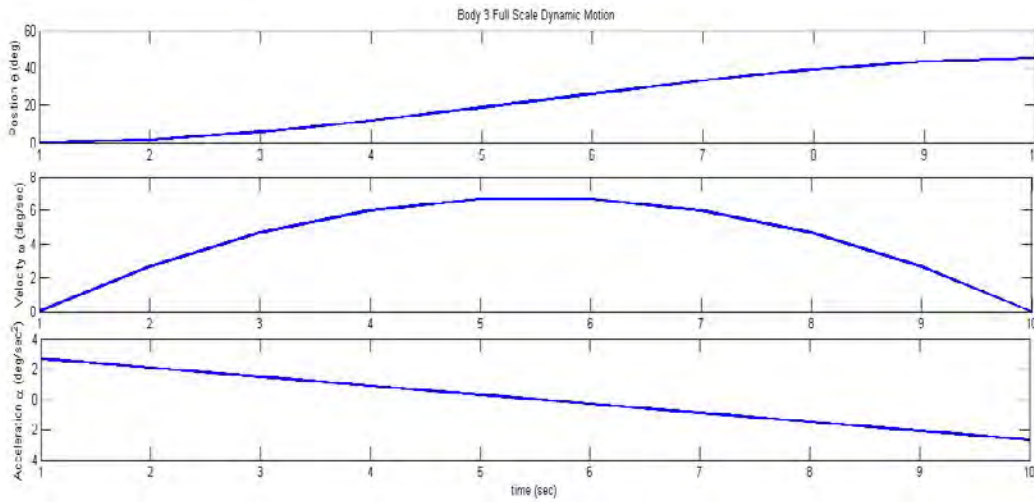

Figure 77.   Body 3 Full Scale Dynamic System States for a 45° Slew
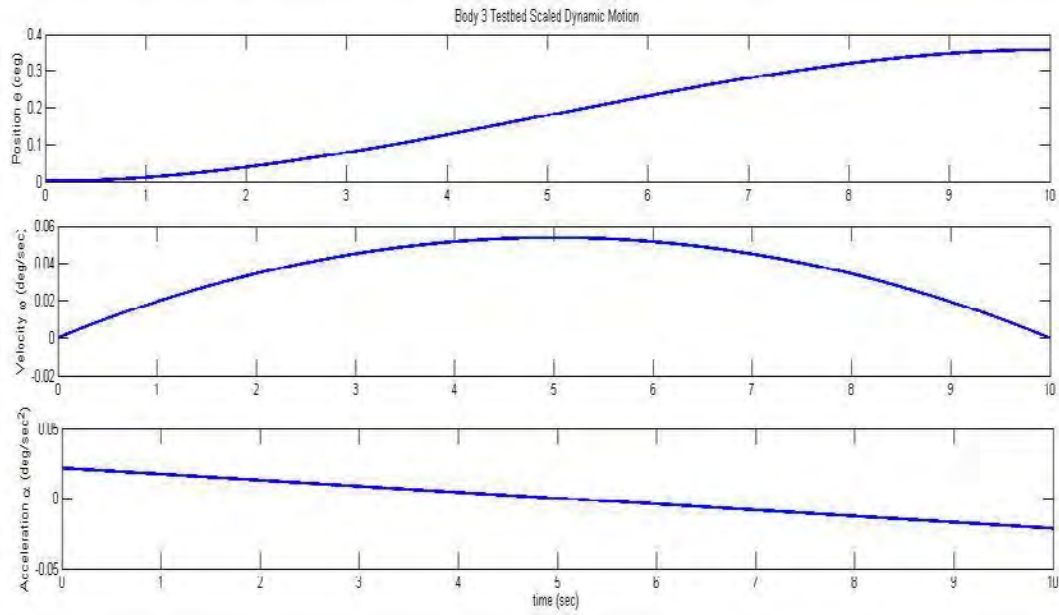
Figure 78.   Body 3 Testbed (Scaled) Dynamic System States
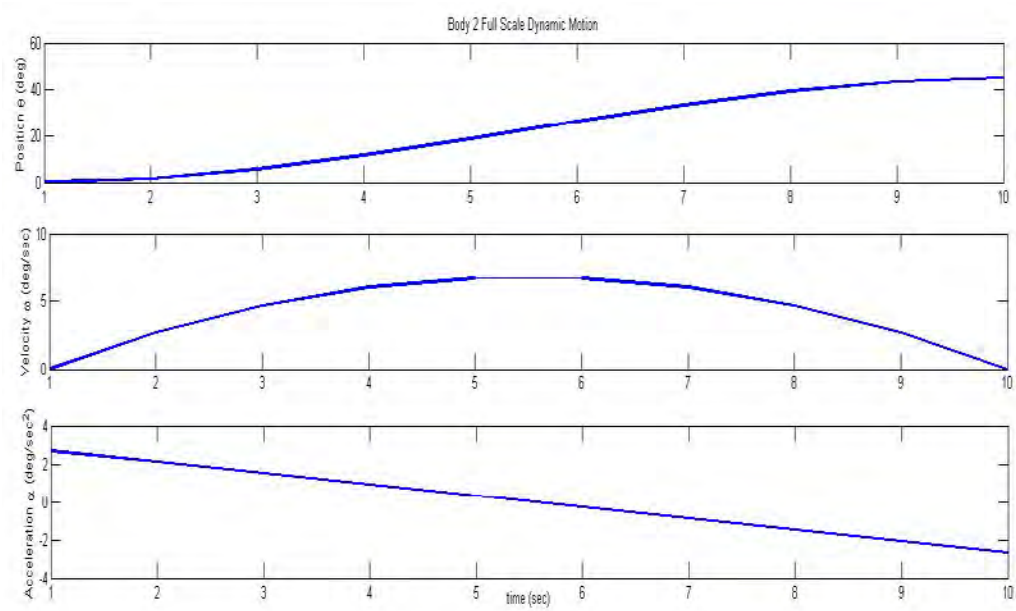
Figure 79.   Body 2 Full Scale Dynamic System States for a 45° Slew
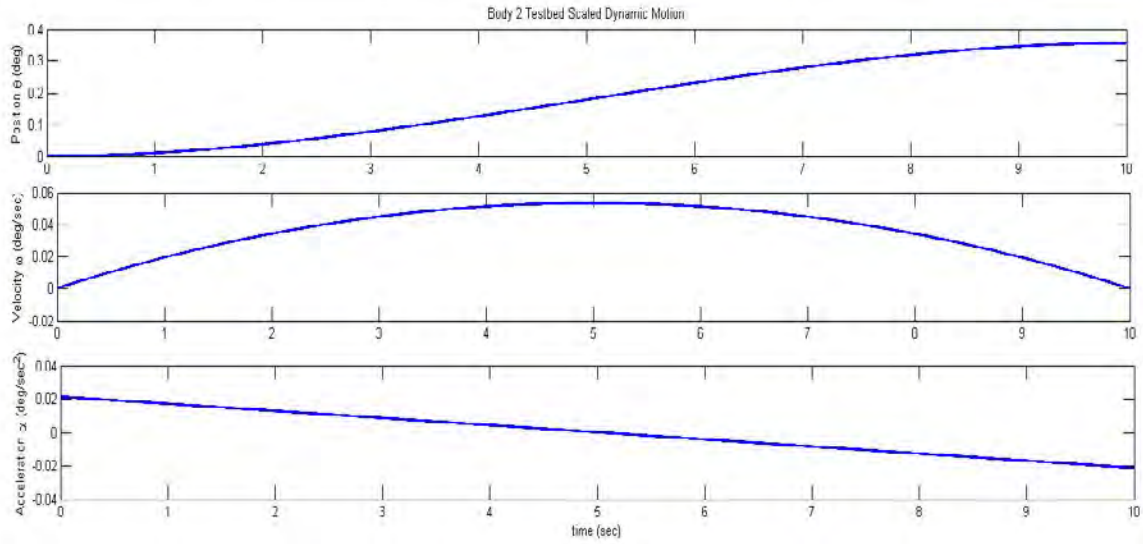
Figure 80.   Body 2 Testbed (Scaled) Dynamic System States

2.   Discussion of Results from Dynamic Scaling Exercise

As mentioned previously, method one is not a practical process to dynamically scale the full scale system to the testbed, but could be used with the understanding that modifying the inertias of the testbed bodies is required. Method two provided useable data to implement on the testbed gimbals. The method two scaled data was reasonable but difficult to implement because the values were small. This suggests that additional mass may need to be added to the system to increase the testbed inertias in order to make it easier to mimic a real world system. The curves shown in Figure 77 to Figure 80 appear to be scaled dynamics, but further experiments on additional full scale systems should be conducted to validate the method.

VI. CONCLUSION

A. CONCLUSIONS

This thesis contributed to the testing of antenna slewing systems by designing and building a testbed antenna assembly, which is fully operable. The testbed assembly was successfully designed, manufactured and tested, and can be used to do a variety of tests on antenna systems aimed at improving the efficiency of these systems. Moreover, the final result meets requirements of quick build, scalable antenna system and arbitrary input maneuvers. This was done using rapid prototyping, the iterative design process, and market research.

Despite the success of the thesis, the design of a testbed that required COTS equipment was not an easy task. Throughout the process there were delays in requisitioning parts for the testbed. Due to the delays, alternate designs such as the AZ gimbal were manufactured in lieu of purchasing an azimuth bearing table. It is recommended that future researchers looking to purchase parts, specifically expensive flight hardware or high precision equipment do so in timely manner and develop alternate designs in the chance the parts do not arrive in time, as was the case with this testbed.

Additionally, during the research of motor control software, it was claimed by Maxon and NI that the LabVIEW and EPOS2 systems would work as a plug-n-play system. This was not the case! It took lengthy amount of time to learn to use the LabVIEW software and implement the cRIO application system. The cRIO implementation and utilizing the EPOS2 drivers onto LabVIEW took nearly two months away from possible design changes and testing. Though the EPOS2 drivers on LabVIEW did eventually work, it still forced the author to research other methods of operating the Maxon motors to ensure multiple-axis motion could be realized.

B.   FUTURE WORK

1.   Nelson Air Bearing

During the market research for possible gimbal motors, the opportunity arose to purchase a Nelson air bearing table as solution for the azimuth axis. The air bearing met the requirements listed in Chapter II and was programmable through LabVIEW. The bearing is highly recommended by the author as a replacement for the current azimuth assembly, replacing the base, gears and AZ motor. The bearing is recommended because it can also be controlled using LabVIEW software, meets the gimbal requirements for speed and position, and reduces the errors associated with using 3D printed parts. A deck plate would need to be designed to attach the shaft and EL gimbal assembly to the air bearing and new inertia data would have to be calculated for future experiments. Many other air and mechanical bearings are available as COTS equipment and should be considered prior to having the need to design and manufacture in-house.

2.   Multiple Motors Using Master Encoder Mode

When researching equipment that could operate multiple motors simultaneously, Maxon recommended the Master Encoder Mode. Master encoder mode allows an EPOS2-P (programmable) motor controller to command an EPOS2 motor controller via encoder outputs [16]. EPOS studio 2.0 has a master encoder mode, which the author implemented with an EPOS2 and EPOS2-P (as the master driver) and custom wiring. Using master encoder mode is important because it provides the gimbals an additional motor (slave) to rotate in the same or opposite direction as the master motor. The master encoder setup can be used as future work for adding a third or fourth motor to provide axial support of a larger gimbal load. Large gimbal loads could be anything attached to the EL or AZ gimbals that would require more torque than any single motor could output (like a larger antenna dish on the EL gimbal). The slaved motor can operate in the same direction as the master or in opposite polarity of the master (if the motors face each other), the EPOS Studio also allows the slaved motor to operate at a reduced speed of the master. The reason for not utilizing master encoder mode is that the EPOS2-P drivers do not exist for LabVIEW; therefore, it was not possible to use the LabVIEW architecture

88

during this thesis. This may change as LabVIEW is further developed. The master encoder mode was setup in accordance with reference [16]. Of note, the setup using EPOS 2.0 studio was important to establish initial communications with EPOS2 controllers, initial calibrations on motors and understand setup behavior for the motors.

3. Case Studies

One of the reasons for building the testbed was to provide an approach to testing a system with azimuth and elevation gimbals. With an operational testbed, it is a matter of future research to design additional prototypes with the approaches provided in this thesis. There exist other applications for which to use the testbed or use some variant of the design. Some antenna system examples that were alluded to in Chapter II are: LANDSAT, sea systems like CIWS, on-orbit NASA antenna systems, and NASA ground systems. In addition to antenna systems, future variants of the testbed could be designed without a dish and the elevation gimbal can be replaced with any end effector design, such as: telescopes, radar systems such as Cobra Judy Replacement, robotic humanoid heads, or even weapon systems.

Independent of the design, the utilization of the Maxon and LabVIEW real-time system could provide a variety of implementation options in future experiments. Previous or future thesis could be engaged with the hardware and software setup developed during this thesis. For example, reference [3] utilizes the Maxon motors but in the research only achieved a design that utilized one motor; with the Maxon-LabVIEW setup a new system could be approached with multiple motors running simultaneously with different trajectories. Another use for the gimbals is to test trajectory paths constructed from optimal control experiments. The optimal control experiment can come from any of the antenna systems listed above.

4. Future Designs

The testbed design went through several iterations, as discussed in Chapter III. However with the short timeline, a design (prototype one) was needed to conduct tests. Other designs were considered, but the author did not have enough time to design, build and test. Optional or future designs that were discussed but not utilized were: 1)

Eliminating the gooseneck from the testbed; this would align the azimuth and elevation axis on the same plane. This design would put the T-frame on top of the gooseneck adapter plate and aligning the motor outputs, as well as reducing the moment created along the length of the gooseneck as shown in Figure 81; 2) Eliminate the large testbed and design a small platform that contains a motor (no gears) that mates to another small housing for an elevation gimbal, as illustrated in Figure 82; 3) Modify the designed base and gear support block to include thrust bearings to improve the azimuth gimbal operation.
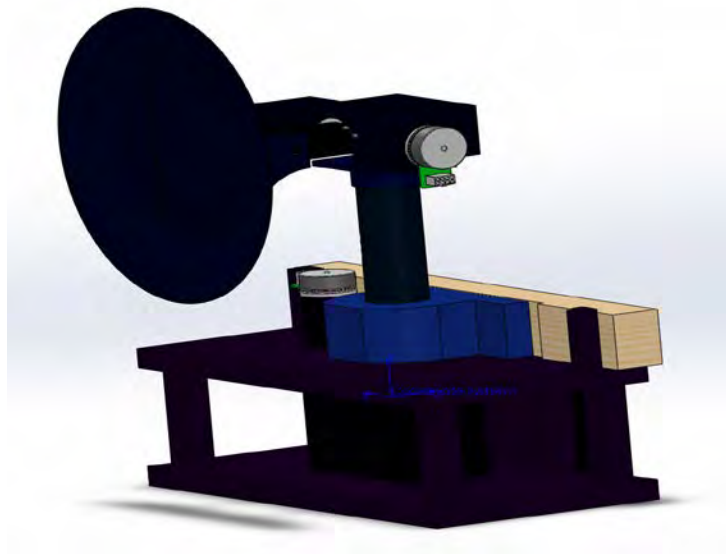

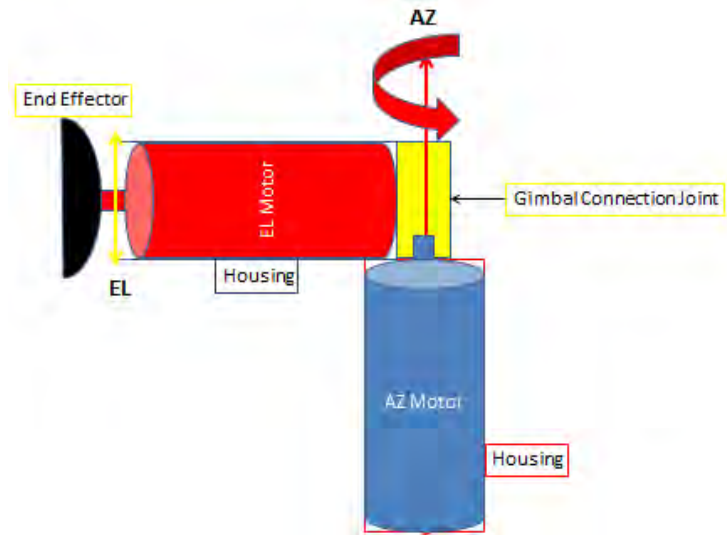Figure 81.   Possible Future Design without Gooseneck

Figure 82.   Possible Future Testbed Design

THIS PAGE INTENTIONALLY LEFT BLANK

LIST OF REFERENCES

[1]   P. Pae, "Satellites' longevity limits sales," *Los Angeles Times*, Los Angeles, CA, December 01, 2008.

[2]   T. K. Bateman, "Design and laboratory implementation of autonomous optimal motion planning for non-holonomic planetary rovers," M.S., Monterey, CA Naval Postgraduate School, 2012.

[3]   K. L. Ackman, "Prototyping of an open-architecture CMG system," M.S., Monterey, CA, Naval Postgraduate School, 2012.

[4]   World Technology Evaluation Centers, "Rapid Prototyping in Europe and Japan," Loyola College, Baltimore, 1997.

[5]   D. Sakoda, "3D Printing Home (3D Geometry Printed in Plastic)," Naval Postgraduate School, 2013. [Online]. Available: https://wiki.nps.edu/display/ SSAGRP/3D+Printing+Home+%283D+Geometry+Printed+in+Plastic%29. [Accessed 2013].

[6]   W. Witaya, "Scaled Vehicle for Interactive Dynamic Simulation," in *International Conference on Robotics and Biomimetics*, Bangkok, 2009.

[7]   D. W. Repperger, "Dynamic scaling of one-seventh size F-15 prototypes," Air Force Materiel Command, Wright Patterson Air Force Base, OH, 1995.

[8]   R. Smith and S. D. Eppinger, "Identifying controlling features of engineering design iteration," Management Science, vol. 43, pp. 276–293, 1997.

[9]   Stratasys, "PC (polycarbonate) Production-Grade Thermoplastic for Fortus 3D Production Systems," 2013. [Online]. Available: www.stratasys.com.

[10]   R. L. Norton. *Design of Machinery* (3rd. ed.), Worchester, MA: McGraw-Hill, 2004.

[11]   Padmaraja Yedamale, Microchip Technology Inc., "Brushless DC (BLDC) motor fundamentals," Microchip Technology Inc., Chandler, AZ, 2003.

[12]   Maxon Motors, "Maxon Motors USA," Maxon Motors, 2013. [Online]. Available:http://www.maxonmotor.com/maxon/view/product/gear/planetary/gp42 /203126.

[13]   Maxon Motor, *Maxon academy: Practical training with the EPOS studio* [Technical Manual]. Sachseln: Maxon Motor ag, 2010.

[14] Maxon Motor, "EPOS positioning controllers: application notes collection," *[Technical Manual],* 2012.

[15] National Instruments, "Controller area network," 2013. [Online]. Available: www.ni.com/can.

[16] Maxon Motor USA, *EPOS2 Programmable Positioning Controller* [Technical Manual]. Sachseln: Maxon Motor ag, 2012.

[17] CAN in Automation e.V., "CAN CiA," CAN in automation e.V., 2013. [Online]. Available: http://www.can-cia.org/.

[18] Maxon Motor, *EPOS Positioning Controller: Documentation for Windows 32-Bit DLL* [Technical Manual]. Sachseln: Maxon Motor ag, 2007.

[19] National Instruments, "NI SoftMotion Axis Interface for EPOS2 Positioning Controller maxon motor," NI and Maxon Motor, 2010. [Online]. Available: http://sine.ni.com/nips/cds/view/p/lang/en/nid/209755.

[20] National Instruments, "www.ni.com," National Instruments, 2013. [Online]. Available: http://www.ni.com/compactrio/.

[21] I. M. Ross, *A Primer on Pontryagin's Principle in Optimal Control.* San Francisco: Collegiate Publishers, 2009.

[22] M. Ahmad, J. D. Jiya, E. C. Anene, Y.S. Haruna, "Position control of parabolic dish antenna using feedback, Zeigler-Nichols and quadratic optimal regulator methods," *Wilolud Journals*, vol. 6, no. 3, pp. 7–13, 2011.

[23] Dassault Systèmes, "SolidWorks Fundamentals, Measurement, and Mass Properties and Section Properties," Dassault Systèmes, 2013. [Online]. Available: http://help.solidworks.com/2011/english/SolidWorks/sldworks/legacyhelp/sldworks/parts/HIDD_MASSPROPERTY_TEXT_DLG.htm.

[24] E. Stoneking, "Newton-Euler Dynamic Equations of Motion for a Multi-body Spacecraft," NASA Goddard Space Flight Center, Greenbelt, MD, 2007.

[25] A. G. Sears, "Design and Experimental Implementation of Optimal Spacecraft Antenna Slews," M.S., Monterey, CA, Naval Postgraduate School, 2013.

[26] Hughes Aircraft Company, "Tracking and data relay satellite system," National Technical Information Service, El Segundo, CA, 1972.

[27] TRW Defense and Space Systems Group, "Design study for LANDSAT-D attitude Control System." NASA Goddard Space Flight Center, Greenbelt, MD, 1977.

INITIAL DISTRIBUTION LIST

1. Defense Technical Information Center
   Ft. Belvoir, Virginia

2. Dudley Knox Library
   Naval Postgraduate School
   Monterey, California